REPORT DOCUMENTATION PAGE

Form Approved
OMB No. 0704-0188

1. REPORT DATE	2. REPORT TYPE	3. DATES COVERED *(From - To)*
06 May 2021	Technical Paper	25 March 2021 - 30 May 2021

4. TITLE AND SUBTITLE
CROSSLINK DENSITY MEASUREMENT BY THE DYNAMIC MICRO-INDENTATION METHOD

5a. CONTRACT NUMBER
FA9300-19-C-0003

5b. GRANT NUMBER

5c. PROGRAM ELEMENT NUMBER

6. AUTHOR(S)
Franklin C Wong, PhD

5d. PROJECT NUMBER

5e. TASK NUMBER

5f. WORK UNIT NUMBER
Q1Y8

7. PERFORMING ORGANIZATION NAME(S) AND ADDRESS(ES)
Piezo-Metrics Inc. dba Micron Instruments
4509 Runway St.
Simi Valley, CA 93063-3479

8. PERFORMING ORGANIZATION REPORT NUMBER

9. SPONSORING/MONITORING AGENCY NAME(S) AND ADDRESS(ES)

Air Force Research Laboratory (AFMC)
AFRL/RQRM
4 Draco Drive
Edwards AFB, CA 93524-7160

10. SPONSOR/MONITOR'S ACRONYM(S)

11. SPONSOR/MONITOR'S REPORT NUMBER(S)

AFRL-RQ-ED-TP-2021-075

12. DISTRIBUTION/AVAILABILITY STATEMENT
Distribution Statement A: Approved for Public Release; Distribution is Unlimited. PA Clearance Number: 21238; Clearance Date: 05 May 2021.

13. SUPPLEMENTARY NOTES
The U.S. Government is joint author of the work and has the right to use, modify, reproduce, release, perform, display, or disclose the work.

14. ABSTRACT
The prediction and assessment of SRM service life estimate (SLE) based on measurement of propellant properties using samples from dissected in-service or companion motors is recognized to be a time-consuming and costly endeavor. The measurement of crosslink density using a dynamic micro-indenter was investigated because it may offer a way to eventually measure crosslink density changes in-situ in a solid rocket motor.
Inert propellant slabs, prepared under contract by Northrop Grumman Innovation Systems for crosslink density measurements, were stored in an oven set at 140 F and withdrawn at the prescribed time intervals. Each test specimen was tested at 20 C, 40 C and 60 C using the dynamic micro-indenter method. The indenter frequency was swept between 1 Hz and 100 Hz in seven equal increments in log frequency space over a minimum of seven test locations on the specimen at each temperature.
Statistical analyses showed that there were storage modulus differences among the 0 day, 7 day, 15 to 20 day, 40 to 100 day and 120 day accelerated aging datasets. The inert propellant hardened from 0 to 100 days aging and then softened at 120 days of aging. The crosslink density calculations based on the measured storage moduli determined the crosslink density at 20 C at 0 day aging was 508 mol/m3. After 7 days of accelerated aging, the crosslink density increased to 632 mol/m3. The crosslink density increased to 769 to 824 mol/m3 after 15 to 20 days of aging. After 40 to 100 days of aging, the crosslink density increased further to 892 to 947 mol/m3. The crosslink density decreased to 824 mol/m3 after 120 days of aging. It is recommended that equilibrium swelling measurements or traditional dynamic mechanical analysis be used to confirm these crosslink density results.

15. SUBJECT TERMS
N/A

16. SECURITY CLASSIFICATION OF:			17. LIMITATION OF ABSTRACT	18. NUMBER OF PAGES	19a. NAME OF RESPONSIBLE PERSON
a. REPORT	b. ABSTRACT	c. THIS PAGE			James Singleton
Unclassified	Unclassified	Unclassified	SAR	79	19b. TELEPHONE NUMBER *(Include area code)* N/A

CROSSLINK DENSITY MEASUREMENT BY THE DYNAMIC MICRO-INDENTATION METHOD

Theory and Results

FC Wong

Micron Instruments
4509 Runway St.
Simi Valley, CA 93063

January 2021

Terms of Release:

Micron Instruments

Contract Report

Micron CR 2021-001

This work was performed at Micron Instruments between August 2020 and December 2020 for Contract FA9300-19-C-0003, Subtopic 5 Sensor Technology Development for Solid Rocket Motors under Broad Agency Announcement Motor Aging and Surveillance Technology (BAA MAST) Call 3 (BAA-RQR-2014-0002) Aging and Surveillance (A&S) Technology Development.

Abstract

The prediction and assessment of SRM service life estimate (SLE) based on measurement of propellant properties using samples from dissected in-service or companion motors is recognized to be a time-consuming and costly endeavor. The measurement of crosslink density using a dynamic micro-indenter was investigated because it may offer a way to eventually measure crosslink density changes in-situ in a solid rocket motor.

Inert propellant slabs, prepared under contract by Northrop Grumman Innovation Systems for crosslink density measurements, were stored in an oven set at 140 F and withdrawn at the prescribed time intervals. Each test specimen was tested at 20 C, 40 C and 60 C using the dynamic micro-indenter method. The indenter frequency was swept between 1 Hz and 100 Hz in seven equal increments in log frequency space over a minimum of seven test locations on the specimen at each temperature.

Statistical analyses showed that there were storage modulus differences among the 0 day, 7 day, 15 to 20 day, 40 to 100 day and 120 day accelerated aging datasets. The inert propellant hardened from 0 to 100 days aging and then softened at 120 days of aging. The crosslink density calculations based on the measured storage moduli determined the crosslink density at 20 C at 0 day aging was 508 mol/m^3. After 7 days of accelerated aging, the crosslink density increased to 632 mol/m^3. The crosslink density increased to 769 to 824 mol/m^3 after 15 to 20 days of aging. After 40 to 100 days of aging, the crosslink density increased further to 892 to 947 mol/m^3. The crosslink density decreased to 824 mol/m^3 after 120 days of aging. It is recommended that equilibrium swelling measurements or traditional dynamic mechanical analysis be used to confirm these crosslink density results.

Table of contents

List of Figures

List of Tables

Acknowledgements

The author would like to acknowledge the support from James Singleton, Group Lead – SRM Aging and Surveillance, Solid Rocket Motors Branch, AFRL Aerospace Systems Directorate, Edwards AFB.

1. INTRODUCTION

The standard industry practice to predict and determine solid propellant rocket motor (SRM) service life has been to conduct, during the design stage, a structural analysis of the propellant grain under the most severe environmental and firing condition(s) expected, and apply safety factors based on the available mechanical properties of the unaged and accelerated aged propellant. Then, on a periodic basis, withdraw a sample of SRMs, dissect them, characterize the chemical and mechanical properties of the naturally-aged propellant and other structural materials and perform detailed structural analysis to calculate the probable service life of the SRM design.

It is recognized that prediction and assessment of SRM service life estimate (SLE) based on measurement of Propellant-Liner Interface (PLI) and propellant properties using samples from dissected in-service or companion motors is both a time-consuming and costly endeavor. Moreover, the time and expense of motor dissection often severely limits the number of specimens that are machined for material property testing. As a result, the statistical uncertainties in the measured material properties within a motor and within a fleet of motors are relatively high due to the low number of available samples. This statistical uncertainty directly impacts the predictive capability of the selected service life prediction method. It has been shown that the confidence-interval-width (CIW) is inversely proportional to the root of the sample size[1]. So, if the sample size can be increased from three measurements to just seven measurements, the CIW can be reduced by 34%.

Past government-sponsored efforts like the Sensors Application and Modeling (SAM) program, the RQRP Embedded sensor development program and the AMPT TO5 program developed sensor technologies that reduced the uncertainties by directly measuring input parameters used in the SLE assessment method. Since the measurements are made in-situ, the sensors offered a way to increase the sample size of the measurements as well. Continuing with this approach, if the variance in the propellant properties can be measured in-situ with greater frequency to reduce statistical uncertainty and the SRM PLI condition can be measured in-situ with greater frequency to reduce uncertainty in the stresses acting on the interface, the Aging and Surveillance Technology Development requirements of: 1) reduced predictive uncertainty of service life estimates for SRM, and 2) reduced reliance on motor dissection, is achievable.

The measurement of the PLI properties was studied in [1] and [2]. A Normal Shear Stress and Temperature (NSST) sensor was designed and fabricated and the method to calibrate it was developed. To address the material property measurement of solid propellant,

[1] http://sphweb.bumc.bu.edu/otlt/mph-modules/bs/bs704_confidence_intervals/bs704_confidence_intervals_print.html, accessed 18 Sep 2017.

Micron Instruments proposed the investigation of an in-situ non-destructive method to measure the crosslink density of the propellant binder.

Crosslink density has been calculated using dynamic modulus data measured with costly dynamic mechanical analyzers (DMA). However, the DMA cost and sample preparation requirements limit the number of samples that can be tested within a given timeframe. A theoretical basis exists to calculate a propellant's storage modulus and crosslink density from the oscillatory force-displacement data using an indenter. Measuring dynamic modulus using an indenter on small propellant samples is expected to reduce test specimen preparation time and sensitivity to imperfect test boundary conditions. If the technique is successful, the concept may be extendable to the development of an in-situ crosslink density measurement sensor that can accurately and precisely characterize the aging behavior of the propellant in solid rocket motors.

This report documents the measurement of crosslink density using the dynamic micro-indentation method. Section 2 summarizes previous studies using dynamic micro-indentation to measure mechanical properties. Section 3 presents the theory supporting the measurement of crosslink density using dynamic micro-indentation. Section 4 describes the development of the inert propellant used in this study. Section 5 details the dynamic micro-indenter test method. Section 6 presents the preliminary tests used to verify the dynamic micro-indenter method. Section 7 presents the test results for the accelerated aged inert propellant. Section 8 details the crosslink density results of the accelerated aged propellant.

2. BACKGROUND

Solid propellant is comprised of oxidizer particles that are held together by a hydrocarbon binder among other constituents to form a self-contained fuel source [3]. Failure of the solid propellant can occur due to chemical and mechanical degradation. Chemical degradation may take the form of plasticizer loss, stabilizer loss or crosslink change in the polymer network [4]. Mechanical degradation at a mesoscopic level can be attributed to weakening of the oxidizer-binder bond [5].

Given the high solids loading in solid propellants, changes in the crosslink density of the binder may be an important indicator of material degradation. Past studies have measured crosslink density through solvent infusion [6], dynamic mechanical analysis (DMA) and nuclear magnetic resonance [7].

In 2007, El-Sabbagh [8] compared the results of three different methods that measure crosslink density. The three methods were: 1) differential torque [9], 2) equilibrium volume swelling [6], and 3) mechanical shearing [7]. The theoretical basis for characterizing crosslink density by mechanical shearing was outlined by Treloar [10]. Treloar derived the relationship between shear modulus, G, and average chain molecular weight, Mc, to be

$$G = \rho R_c T / M_c \tag{1}$$

where G is shear modulus (Pa),
ρ is density of the material (kg m^{-3}),
R_c is universal gas constant (8.314 m^3 Pa K^{-1} mol^{-1}),
T is absolute temperature (K),
M_c is average chain molecular weight (kg mol^{-1}).

Therefore, if the shear modulus of a polymer can be measured, the average chain molecular weight can be calculated and related to crosslink density through the relation

$$\gamma = \frac{\rho}{M_c} \tag{2}$$

where γ is crosslink density (mol m^{-3}),
ρ is density of the material (kg m^{-3}).

Figure 1 shows a comparison of the crosslink density measurements El-Sabbagh obtained using the swelling and mechanical shearing techniques for different blends of cured natural rubber (NR), styrene-butadiene rubber (SBR) and nitrile rubber (NBR). Mechanical shear was applied using a dynamic mechanical analyzer. Shear storage modulus was measured at the rubbery plateau [11]. As the small percentage difference results in Figure 1 show, the mechanical shearing or DMA method of measuring crosslink density gave similar results as the classical swelling method.

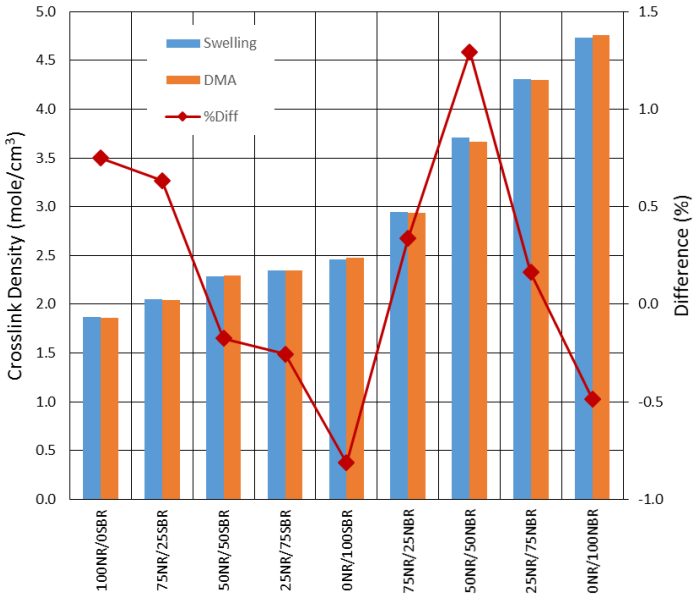

Figure 1: Comparison between crosslink density measured by swelling and DMA [8].

Rather than twisting or pulling a test specimen using the DMA method [12], Czerner [13] used indentation mechanics to characterize nonlinear material properties is an ongoing area of research. Bles [14] described the behavior of polyurethane in terms of the Edwards-Vilgis free energy density function, *W*, which is dependent on four parameters related to crosslink density, entanglement density, entanglement friction and chain locking stretch and the Maxwell-type linear viscoelasticity. Force-depth data collected from cyclically indenting a polyurethane sample with a Vickers indenter was input into an inverse identification algorithm to deduce the constitutive equation parameters including, N^*_c, which is related to crosslink density.

Rather than defining a material's constitutive equation in terms of a structure-property parameter like crosslink density, Lin [15] took a solid mechanics approach and defined the constitutive equation in terms of modulus by extending the Hertzian relationship between applied force and indentation depth to hyperelastic materials. The general form of Lin's force-depth equation was

$$\frac{F}{\pi a^2} = \frac{20E}{3\pi(1-\vartheta^2)} 0.2 \frac{a}{R} \qquad (3)$$

where F = force (N),
E = tensile modulus of material (Pa),
υ = Poisson ratio (-),
a = contact radius (m),
R = spherical indenter radius (m).

The indenter depth was related to the contact radius by

$$a = \sqrt{R\delta} \quad (4)$$

where δ = indenter depth (m). Equation 3 can be expressed in terms of shear modulus, *G*, by employing the elasticity relationship

$$G = \frac{E}{2(1+\vartheta)} \quad (5)$$

The notional equation governing measurement of crosslink density using the force-depth data measured with an oscillating indenter at a material's rubbery plateau temperature is

$$\gamma = \frac{3(1-\vartheta^2)F'}{8\sqrt{R}(1+\vartheta)\rho R_c T\sqrt{\delta^3}} \quad (6)$$

where γ = crosslink density (mol m^{-3}) and F' = storage modulus component of the oscillating force (Pa). The remaining parameters are defined in equations 1 to 5.

Herbert [16] proposed that an indenter could be used to create a strain field in a material sample and that a load cell connected to the indenter could be used to measure the integrated forces exerted by a material on the indenter as means to measure the complex modulus of the material. In [17], Herbert made a side-by-side comparison between the conventional DMA method and a DMA-style indentation method using a flat punch indenter. Herbert showed that the two methods measured the complex modulus of a highly-plasticized thermoplastic to within 15% of each other.

Guglielmi [18] adopted the Herbert's technique to characterize the complex modulus of hydrogels using a nano-indenter. Guglielmi noted that the nano-indentation technique had the following advantages over conventional material characterization methods:

a) nano-indentation is able to test small volumes of materials with spatial resolutions in the nm and μm range,

b) nano-indentation is able to test materials with little surface preparation,

c) nano-indentation is able to control measured or applied force and displacement in the μN and nm range, respectively,

d) nano-indentation is able to characterize materials with a variety of deformation modes by using different time scales, indenter tip geometries and loading conditions.

These studies provide the main motivation to explore the use of nano-indentation to study the aging behavior of solid propellants.

3. THEORY

This Section summarizes the theory supporting the measurement of complex modulus using the dynamic nano-indentation method and the calculation of crosslink density using complex modulus data. The term nano-indentation is replaced by micro-indentation here to acknowledge the higher capacity force actuator used in this study. Nano-indentation is associated with a 50 mN actuator while micro-indentation is associated with a 1000 mN actuator. The theory of operation is identical in both cases.

The theory behind micro-indentation was developed in [21] and [22]. A summary of the theory is provided here for completeness.

Figure 2 shows a schematic of the micro-indenter dynamic system including the contributions of the sample properties (shown in red). The definition of the parameters are as follows:

- K_f is the stiffness of the micro-indenter frame (N/m)
- K_i is the stiffness of the micro-indenter actuator (N/m)
- D_i is the damping coefficient of the micro-indenter actuator (N-s/m)
- m_i is the moving mass of the micro-indenter (kg)
- S is the contact stiffness of the sample under test (N/m)
- D_s is the damping coefficient of the sample under test (N-s/m)
- m_s is the moving mass of the sample under test (kg)
- F(t) is the time-varying applied oscillating force on the sample (N)
- z(t) is the measured time-varying displacement on the sample (m)

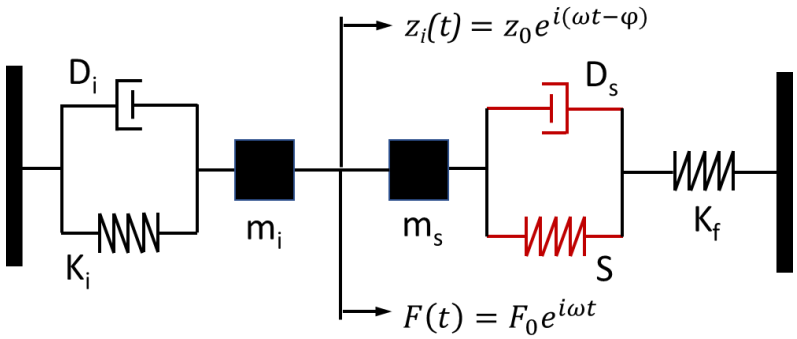

Figure 2: Schematic of indentation system including the sample (S, D_S, m_s) properties.

Note that the complex modulus, E^*, of the sample under test is related to the parameters, S and D_s, the sample contact stiffness and damping coefficient, respectively. In order to measure these parameters, the micro-indenter system properties must be known.

The equation of motion representing the micro-indenter system and sample under test, as shown in Figure 2, is

$$(m_i + m_s)\ddot{z} + (1/D_i + 1/D_s)^{-1}\dot{z} + \left(1/K_i + 1/S + 1/K_f\right)^{-1} z = F_0 e^{i\omega t} \qquad (3)$$

where z is the time-varying displacement (m),
F_0 is the applied force amplitude (N),
ω is the angular rate (r/s),
t is the time (s).

The equation for the time-varying displacement, z, is

$$z(t) = z_0 e^{i(\omega t - \varphi)} \qquad (4)$$

where φ is the phase lag between the applied force and measured displacement,
z_0 is the measured displacement amplitude (m),

The indenter actuator properties, m_i, D_i and K_i are deduced by oscillating the indenter in free-air over a range of angular rates while measuring the applied force, F_0, and displacement, z_0. The equation of motion for a harmonic oscillator freely vibrating in air can be written from eq. 3 and re-arranged to be

$$\frac{z_0}{F_0} = \frac{1}{(K_i - m_i\omega^2)^2 + (D_i\omega)^2} \qquad (5)$$

To deduce the indenter actuator properties, the actuator is oscillated over a range of angular rates, ω_1, ω_2 … ω_n, and the corresponding $(z/F)_1$, $(z/F)_2$ … $(z/F)_n$ data are measured. The $(z/F)_i$ data is plotted against the ω_i data and then an optimization algorithm is applied to determine the values of m_i, D_i and K_i that allow eq. 5 to best fit the n-data points.

The micro-indenter frame stiffness, K_f, must be evaluated experimentally using a Berkovich indenter and a well-characterized material like fused silica [19]. The theoretical basis for the characterization technique makes use of the contact mechanics relationship developed by Sneddon [20] as implemented for micro-indentation experiments by Oliver and Pharr [21], [22].

It can be shown that the overall compliance of the indentation system is given by

$$\frac{1}{K'} = \frac{\sqrt{\pi}}{2E_r}\left(\frac{1}{\sqrt{A}}\right) + \frac{1}{K_f} \qquad (6)$$

where K' is the overall system stiffness (N/m),
E_r is the reduced modulus (MPa),
A is the contact area (m^2).

The hardness, H, is defined as

$$H = \frac{P}{A} \tag{7}$$

where P is the applied force (N),
A is the contact area (m^2).

Substituting eq. 7 into eq. 6 gives the linear equation

$$\frac{1}{K'} = \frac{\sqrt{\pi H}}{2E_r}\left(\frac{1}{\sqrt{P}}\right) + \frac{1}{K_f} \tag{8}$$

where K′ is the measured overall system stiffness of F/z (N/m),
P = F is the applied/measured force (N).

The plot of the measured overall system compliance, 1/K′, versus the applied force, $1/\sqrt{P}$, will be a straight line with its intercept at $1/K_f$.

The complex modulus, E^*, is defined by [16]

$$E^* = E' + E'' \tag{9}$$

where E′ is the storage modulus (Pa),
E″ is the loss modulus (Pa).

The loss factor, tan δ, is defined by

$$\tan\delta = \frac{E'}{E''} \tag{10}$$

From eqs. 3 and 4, the real and imaginary parts of the harmonic oscillator behavior are

$$\left(\frac{1}{K_i} + \frac{1}{K_f} + \frac{1}{S}\right)^{-1} = \frac{F_0}{z_0}\cos\varphi \tag{11}$$

$$\left(\frac{1}{D_i} + \frac{1}{D_S}\right)^{-1}\omega = \frac{F_0}{z_0}\sin\varphi \tag{12}$$

The real component of the complex modulus, E′, is related to the contact stiffness, S, and the imaginary component, E″, is related to the contact damping coefficient, D_s. The two values of S and D_s are solved from eqs. 11 and 12, respectively.

Sneddon [20] showed that the reduced modulus, E_r, in contact mechanics is related to the contact stiffness through eq. 13

$$E_r = \frac{S}{2a} \tag{13}$$

where E_r is the reduced modulus (Pa),
S is the contact stiffness (N/m),
a is the contact radius of the flat punch indenter (m).

The reduced modulus, E_r, is defined by

$$\frac{1}{E_r} = \frac{\left(1-\vartheta_p^2\right)}{E_p} + \frac{\left(1-\vartheta_i^2\right)}{E_i} \tag{14}$$

where E_p is the modulus of the material under test (Pa),
υ_p is the Poisson ratio of the material under test (-),
E_i is the modulus of the indenter (Pa),
υ_i is the Poisson ratio of the indenter (-).

For the material of interest in this study, the modulus of the steel indenter is much greater than the modulus of the material under test. Combining eqs. 9, 11 and 12 to 14 gives [23]

$$E_p' = \frac{S\left(1-\vartheta_p^2\right)}{2a} \tag{15}$$

$$E_p'' = \frac{D_s\omega\left(1-\vartheta_p^2\right)}{2a} \tag{16}$$

The governing equation to measure a polymer's crosslink density using the proposed micro-indentation method is, therefore, calculated by combining eqs. 1, 2, 5 and 15

$$\gamma = \frac{1}{R_cT}\left[\frac{S\left(1+\vartheta_p^2\right)}{4a\left(1+\vartheta_p\right)}\right] \tag{17}$$

where γ is the crosslink density of the material under test (mole/m^3),
R_c is the universal gas constant (8.3143 m^3 Pa kg^{-1} K^{-1}),
T is the absolute temperature during test (K),
ϑ_p is the Poisson ratio of the material under test (-),
S is the contact stiffness (N/m),
a is the contact radius (m).

If the test apparatus software calculates the storage modulus, E', based on the measured contact stiffness and contact radius, the governing equation for crosslink density becomes

$$\gamma = \frac{1}{R_cT}\left[\frac{E'}{2\left(1+\vartheta_p\right)}\right] \tag{18}$$

which recovers the form of eq. 1 except in terms of E′.

4. ACCELERATED AGED INERT PROPELLANT

Investigation of the dynamic micro-indentation method required the availability of a test material with well-characterized aging properties so that the evolution of crosslink density could be measured. To that end, Northrop Grumman Innovation Systems (NGIS) was contracted to develop an inert solid propellant that would age under accelerated aging conditions over an approximate 120 day period at a controlled rate. The statement of work for the NGIS contract is provided in Annex A for reference.

4.1 Propellant Formulation

NGIS proposed a proprietary Hydroxl-Terminated-PolyButadiene (HTPB)-based propellant mixed with an ingredient that they called 'Nanocat' and ammonium sulfate solids to give the desired aging properties. No information about the plasticizer or particle size distribution was provided.

Four pilot pint mixes were prepared to explore the behavior of the material before committing to a full 5 gal. mix. The main mix parameters of interest were 'Nanocat % wt', 'NCO/OH ratio' and 'TMXDI % wt' (Tetramethyl-xylene diisocyanate). The pilot mix formulations are summarized in the shaded cells in Table 1.

Table 1. Pilot and Final Inert Propellant Formulations

Mix #	Nanocat (% wt)	NCO/OH	TMXDI (% wt)
5719061	0.15	0.937	0.834
5719062	0.30	0.937	0.834
5719068	0.15	0.970	0.863
5719069	0.15	1.037	0.923
0920001*	0.15	0.970	0.863
* Formulation selected for final 5 gal. mix.			

4.2 Aging Rates of Pilot Mixes

The aging behavior of the pilot mixes was evaluated at set intervals after being stored at 140 F. Measurements of 'hot Shore A' (measured at 140 F) were made on the propellant slabs to assess their mechanical properties in a quick, non-destructive manner. Once the propellant slabs increased a significant amount in hardness, a portion of the slabs were withdrawn for mechanical property testing at ambient temperature. A limited quantity of uniaxial test specimens was then stamped from the slabs and the 'cold Shore A'

(measured at ambient temperature), initial tangent modulus, true stress and true strain at maximum stress were measured.

Figure 3 to Figure 6 show the hot Shore A, initial tangent modulus, maximum true stress and true strain at maximum stress in graphical form as a function of aging time in days. Pilot mix 5719062 is not shown because the increased quantity of Nanocat did not make a difference in the measured properties.

Looking only at the pilot mix properties in Figure 3, it can be seen that a rapid rise in hot Shore A occurred in the first fifty days of accelerated aging. Afterwards, the hardening slowed and eventually reached a plateau after approximately 100 days. Mix 5719061 (NCO/OH = 0.937) and Mix 5719068 (NCO/OH = 0.970) exhibited similar hardening behavior. Mix 5619069 (NCO/OH = 1.037) hardened much faster than the other two mixes.

In Figure 4, the initial moduli of the Mix 5719061 (NCO/OH = 0.937) and Mix 5719068 (NCO/OH = 0.970) increased quickly in the first 20 days, plateaued between 20 and 40 days before increasing again. Mix 5619069 (NCO/OH = 1.037) steadily increased in stiffness at a higher magnitude than the other two mixes.

In Figure 5, the maximum true stress of the Mix 5719061 (NCO/OH = 0.937) and Mix 5719068 (NCO/OH = 0.970) increased quickly in the first 40 days and slowly increased for the remaining days. Mix 5619069 (NCO/OH = 1.037) increased steadily in maximum true stress at a higher magnitude than the other two mixes.

In Figure 6, the true strain at maximum stress of the Mix 5719061 (NCO/OH = 0.937) and Mix 5719068 (NCO/OH = 0.970) decreased quickly in the first 40 days and slowly decreased for the remaining days. Mix 5619069 (NCO/OH = 1.037) decreased steadily in true strain at a slightly higher magnitude than the other two mixes.

The mechanical properties behavior of the aged pilot mixes at ambient temperature appeared typical for a HTPB-TMXDI-type propellant. Modulus increased and maximum true stress increased with aging while true strain decreased. The zero-aging day values of modulus and maximum true stress were on the low side while the true strain at maximum true stress was on the high side. Since this inert propellant is only used for an aging study, these atypical values were not a concern.

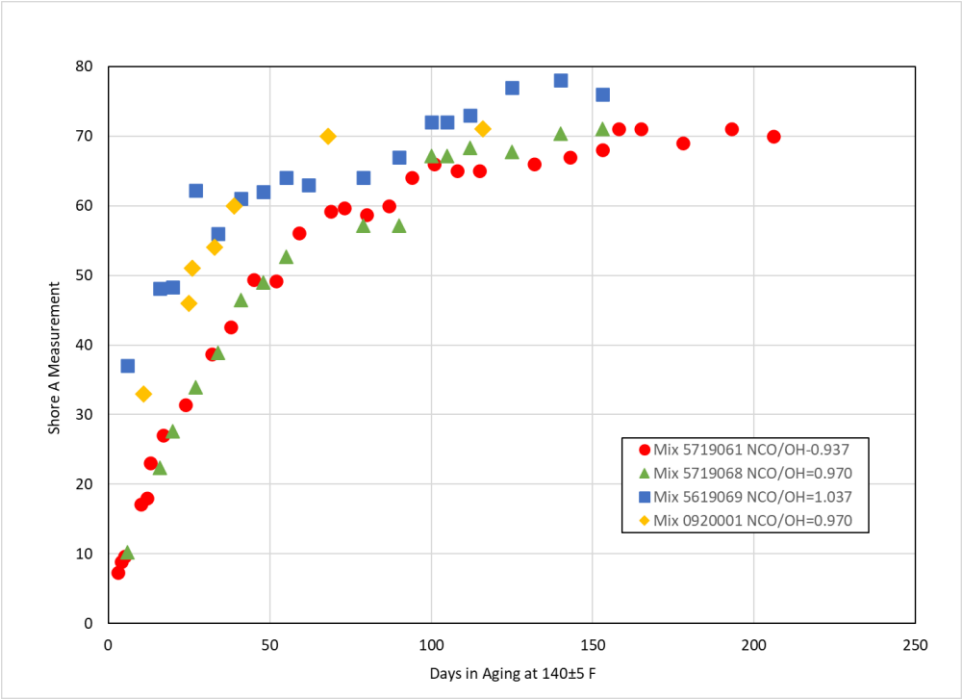

Figure 3: Hot Shore A (measured at 140 F) data for pilot mixes 5719061, 5719068, 5719069 and final mix 0920001.

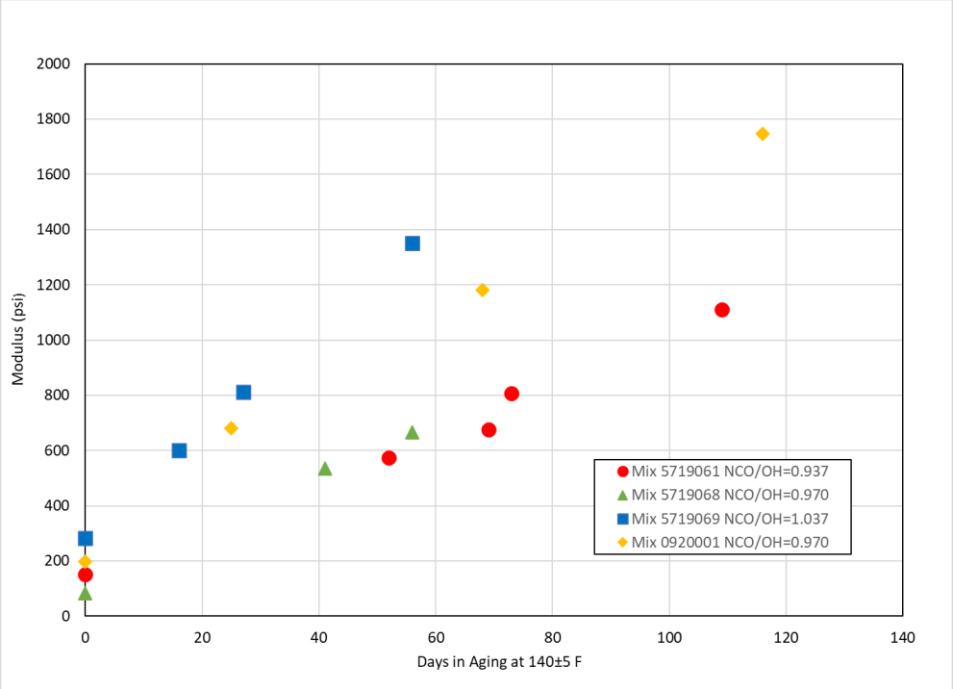

Figure 4: Initial modulus (measured at ambient temperature) data for pilot mixes 5719061, 5719068, 5719069 and final mix 0920001.

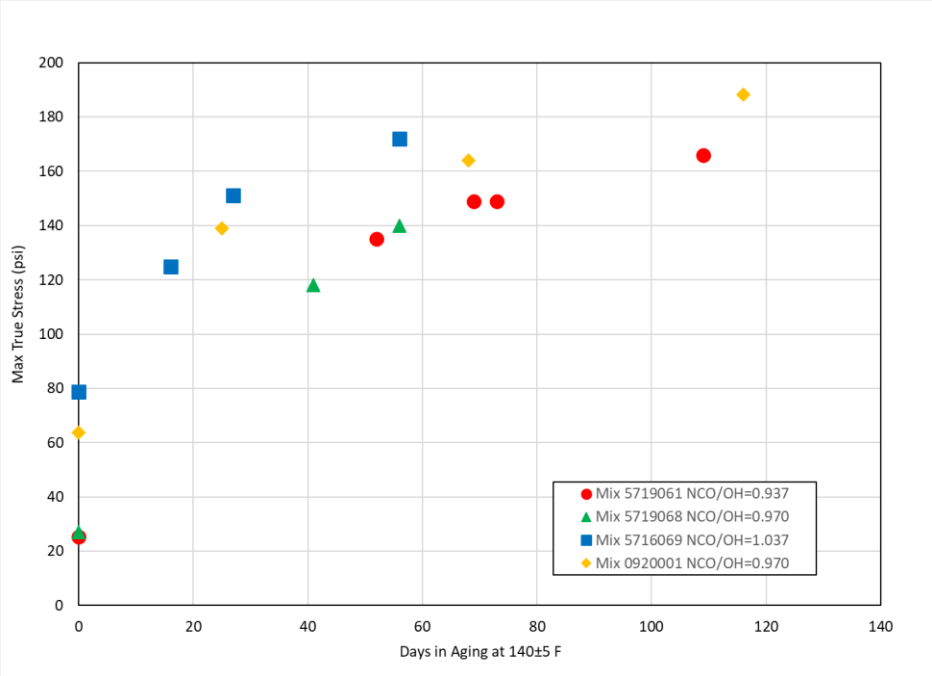

Figure 5: Maximum true stress (measured at ambient temperature) data for pilot mixes 5719061, 5719068, 5719069 and final mix 0920001.

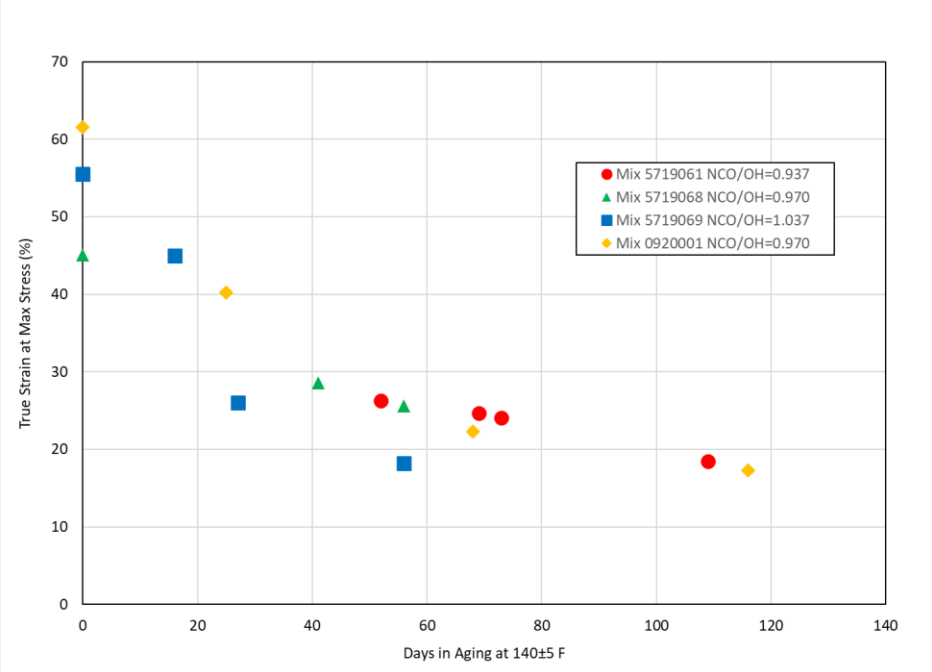

Figure 6: True strain (measured at ambient temperature) at maximum stress data for pilot mixes 5719061, 5719068, 5719069 and final mix 0920001.

4.3 Aging Rate of Selected Formulation

Based on the pilot mix results, the formulation for Mix 5719068 was selected for the final 5 gal. mix. Mix 5719068 had a reasonable increase in modulus over a 100-day period that would allow changes in crosslink density to be measured as eqs. 1 and 2 suggest.

NGIS prepared the final 5 gal. mix according to the formulation shown in Table 1. Pilot and Final Inert Propellant FormulationsTable 1 and named it Mix 0920001. They cut the inert propellant into slabs for an abbreviated aging and characterization study and for shipping to Micron Instruments.

The abbreviated aging study involved measuring the hot Shore A to observe the hardening behavior and to withdraw slabs for uniaxial tensile testing at select times. The results are shown in Figure 3 to Figure 6.

It can be seen in Figure 3 that Mix 0920001 hardened more like Mix 5719069 than Mix 5719068. The initial modulus and the maximum true stress behavior also reflected the properties measured for Mix 5719069. Only the true strain at maximum stress resembled the Mix 5719068 behavior. While the exact cause of this behavior is unknown, it is possible that differences in the chemical kinetics can occur when a mix is scaled up from a pint-size to several gallons.

Table 2 lists the cold Shore A (measured at ambient temperature) of both the pilot and final mixes for reference.

Table 2. Cold Shore* A Measurements

Mix/Days**	**0**	**15**	**30**	**40**	**50**	**60**	**70**	**75**	**110**
5719061	14	---	---	---	66	---	61	68	74
5719068	12	---	---	52	---	52	---	---	---
5719069	48	60	61	---	---	75	---	---	---
0920001***	38	---	56	---	---	---	75	---	71

* Measured at ambient temperature.

** Days of accelerated aging at 140 F.

*** Final 5 gal. mix used for crosslink density study.

4.4 Preparation of Samples for Accelerated Aging

NGIS completed the 5 gal. inert propellant fabrication, cut the propellant into 0.5 in. thick slabs, wrapped them in aluminum foil and plastic wrap and shipped them to Micron Instruments in March 2020. Micron Instruments stored the inert propellant at ambient

temperature until the end of September 2020. In August 2020, slabs were selected for accelerated aging at 140 F according to the schedule shown in Figure 4.

Table 3. Accelerated Aging Schedule and Expected Modulus Increase

Days at 140 F	**Withdraw date**	**Expected increase in modulus**
0	Aug. 26, 2020	1.0 X
7	Sep. 2, 2020	1.5 X
15	Sep. 10, 2020	2.0 X
20	Sep. 15, 2020	2.8 X
40	Oct. 5, 2020	4.0 X
60	Oct. 25, 2020	4.5 X
80	Nov. 14, 2020	5.5 X
100	Dec. 4, 2020	6.5 X
120	Dec. 24, 2020	7.5 X

It was not possible to start accelerated aging of the inert propellant samples in April 2020 because the work with the Normal Shear Stress and Temperature (NSST) sensor calibration was ongoing. Validation of the dynamic micro-indentation method occurred in parallel with the start of accelerated aging at the end of August 2020. The validation effort is presented in Section 6. The aged propellant slabs were stored under vacuum at room temperature in a desiccator to slow any further chemical aging until the inert propellant could be tested.

5. DYNAMIC MICRO-INDENTER METHOD

The micro-indenter system, called the iMicro, was purchased from Nanomechanics Inc., a subsidiary of KLA [24]. A description of the instrument and the dynamic micro-indentation test method is provided in this Section.

5.1 Apparatus

The iMicro instrument is comprised of a highly accurate, one degree-of-freedom harmonic indenter mounted on a Z-axis gantry, a temperature-controlled sample holder, an XY-axis sample positioning stage, a high-resolution video camera, a vibration-isolated, stiff loading frame that mounts the components into position and application software that controls the temperature of the sample holder and operates and acquires data from the instrument (see Figure 7). The operating specifications are summarized in Table 4. The Nanomechanics component list is provided in Annex B.

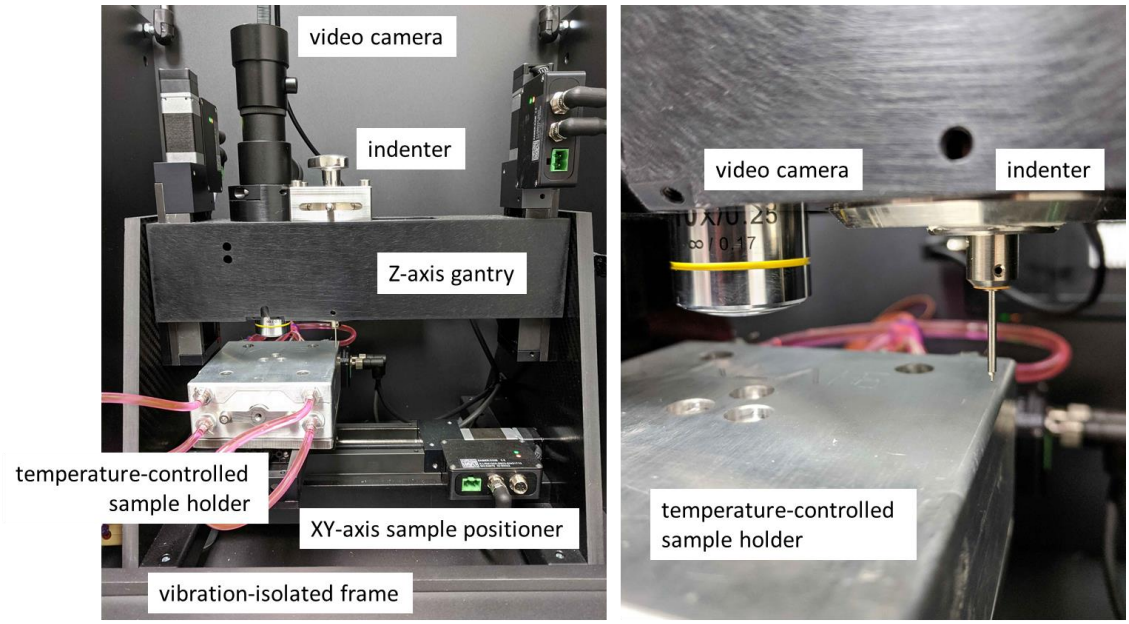

Figure 7: Components in the Nanomechanics iMicro instrument.

The temperature of the sample is regulated by a hot/cold stage sub-assembly. The sub-assembly is comprised of an aluminum glycol-immersion probe-cooled shell, a Thermo Scientific glycol chiller, a Polyscience immersion probe cooler, a BK Precision power supply, an internal electric heater element and a temperature control application (see Figure 8).

Temperature control of the sample is accomplished by first setting the chiller to +18 C or the cooler to –60 C depending on the lowest temperature of interest. The sample temperature is achieved by applying voltage to the internal electric heater until the

desired temperature is reached. The voltage is regulated by a proportional-integral controller using a thermocouple located under the sample for the feedback signal. The proportional value for the controller was set to 0.5 and the integral value was set to 0.01.

Table 4. iMicro System Specifications

Component	**Parameter**	**Value**
Force	maximum force (mN) resolution (nN) noise floor (nN)	1000 6 < 200
Displacement	maximum travel (µm) resolution (nm) noise floor (nm) drift rate (nm/s)	80 0.04 < 0.1 < 0.05
Frequency	range (Hz)	0.1 to 1000
Sample Stage	X-axis maximum range (mm) Y-axis maximum range (mm) Z-axis maximum range (mm)	100 100 25
Frame	stiffness (MN/m)	> 3.5
Controller	data acquisition rate (Hz) control rate (Hz)	1000 500

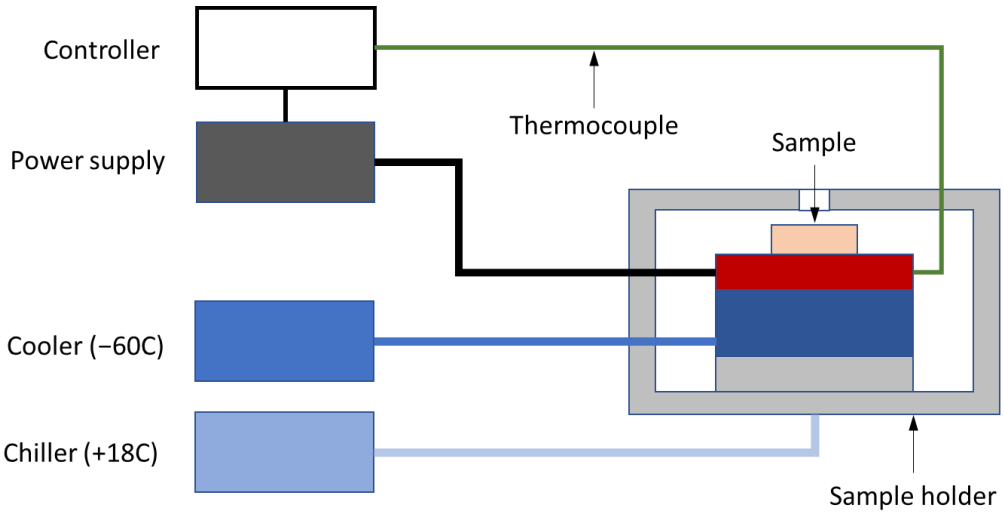

Figure 8: Components of Nanomechanics temperature-controlled sample holder.

5.2 Test Method Sequence

Successful measurement of a sample's complex modulus is highly dependent on the way the iMicro instrument is programmed to operate. The basis for operating the iMicro was first established by Herbert in [16]. The key idea that ensures consistent complex modulus measurement is the reliable detection of the sample surface and the seating of the flat punch indenter into the surface. Table 5 outlines the iMicro operating sequence.

Table 5. iMicro System Operating Sequence

Sample Conditioning
Step 1 – Set desired temperature on controller
Surface Detection
Step 2 – Stabilize actuator position
Step 3 – Lower indenter at fast rate to pre-approach extension
Step 4 – Lower indenter at slow rate for surface detection
Step 5 – Oscillate indenter resonant frequency
Step 6 – Detect surface by reduction in indenter oscillation frequency
Indenter Seating
Step 7 – Upon surface detection, apply surface pre-compression
Step 8 – Measure sample creep rate for data correction
Indenter Frequency Sweep
Step 9 – Calculate oscillation frequency increments based on minimum and maximum frequencies and number of increments
Step 10 – Step through frequency increments by applying indenter force and measuring indenter displacement
Step 11 – Record indenter force and displacement data during oscillations
Calculations
Step 12 – From indenter force and displacement data, calculate surface stiffness and damping coefficient
Step 13 – From surface stiffness and dissipation values, calculate sample storage and loss modulus and loss factor

5.3 Test Method Values

There are a wide variety of test values that need to be set for the test method to function properly. Nanomechanics provided the method entitled ‘'Probe DMA-Complex Modulus-Phase Angle Contact.nmt’ that they successfully used for biological materials [25].

The ‘ProbeDMA-Complex Modulus-Phase Angle Contact.nmt’ method was a starting point for determining the test values that were appropriate for the inert propellant used in this study. After experimenting with a variety of test values on spare samples of inert propellant, the values shown in Table 6 were chosen for use.

Table 6. Values Used in Test Method

Parameter	**Value**
Flat punch diameter (μm)	53.1
Phase change for contact (deg)	8
Surface pre-compression (μm)	1
Dynamic force (μN)	50
Maximum dynamic displacement (nm)	200
Creep determination time (s)	30
Creep tolerance (nm/s)	0.5
Waves to average dynamics (-)	5

6. VERIFICATION OF DYNAMIC MICRO-INDENTER METHOD

The inert propellant fabricated in Section 4 has a non-homogenous structure that adds an additional layer of complexity to the dynamic modulus measurement. To simplify the verification of the dynamic micro-indenter method, neoprene, which is a homogenous polymer, was used to verify the test method. To that end, Warco Biltrite commercial neoprene 1/16 in. thick sheet stock with Shore A values of 30, 50, 60 and 70 was purchased [26].

Each Shore A sheet stock was cut into a 10 mm x 25 mm sample. The sample was installed in the sample holder and conditioned for a minimum of 20 min. to allow it to reach thermal equilibrium. The temperature controller has a control tolerance of +/-1 C. The samples were tested at 20 C, 40 C and 60 C. A frequency sweep between 0.1 Hz and 100 Hz in 9 equal increments in log frequency space was carried out over a minimum of six locations on the sample. Each temperature created a complex modulus dataset as a function of frequency.

The data in each dataset was reduced by averaging the storage modulus, loss modulus and loss factor results from all locations at each frequency. The averaged storage modulus results are presented here. To provide a reference point for visual comparison, unpublished storage modulus data for a filled-HTPB is shown along with the measured storage modulus results. For additional information about the filled-HTPB data, see Annex C.

6.1 Neoprene A30 Results

The master curve in the frequency domain for the neoprene with a Shore A30 is shown in Figure 9. The shift factors are shown in Figure 10. The filled-HTPB master curve and Williams-Landel-Ferry (WLF) curve are provided for reference.

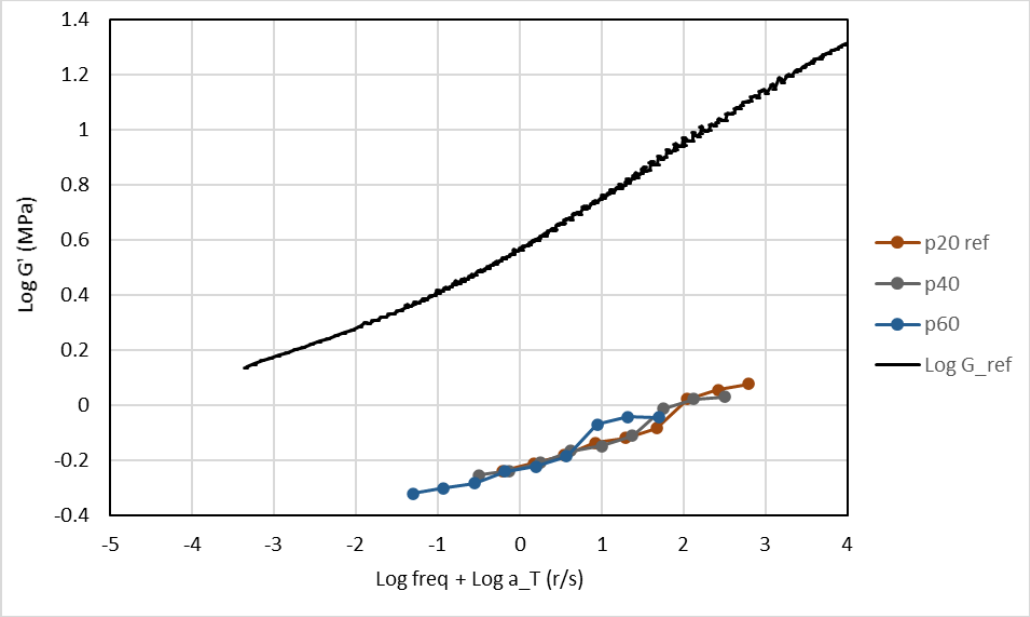

Figure 9: Master storage modulus curve for A30 neoprene compared to master curve for filled HTPB (Log G_ref).

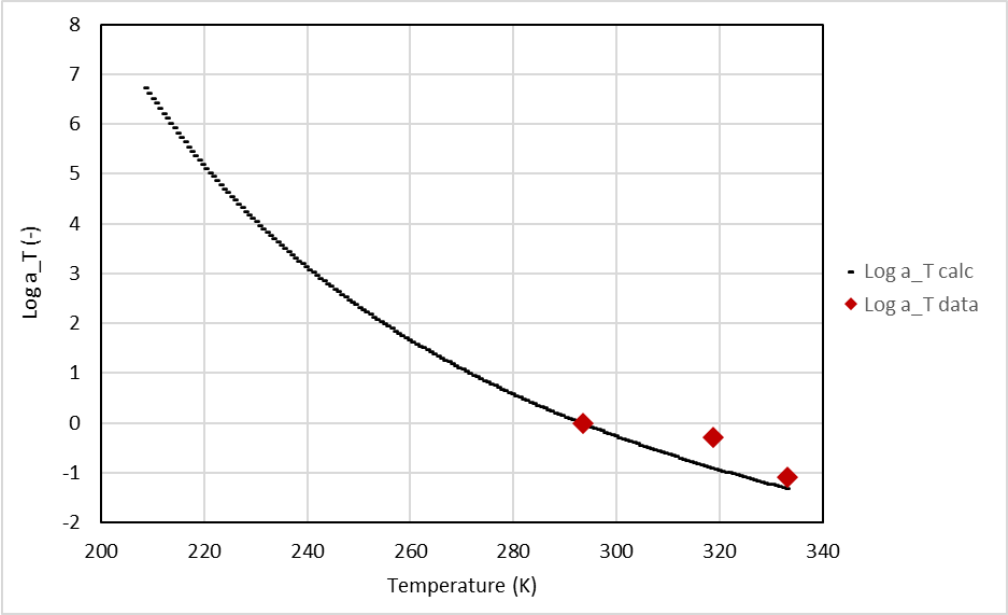

Figure 10: WLF shift factors for A30 neoprene compared to shift factors for filled HTPB (Log a_T calc).

6.2 Neoprene A50 Results

The master curve in the frequency domain for the neoprene with a Shore A50 is shown in Figure 11Figure 9. The shift factors are shown in Figure 12Figure 11. The filled-HTPB master curve and Williams-Landel-Ferry (WLF) curve are provided for reference.

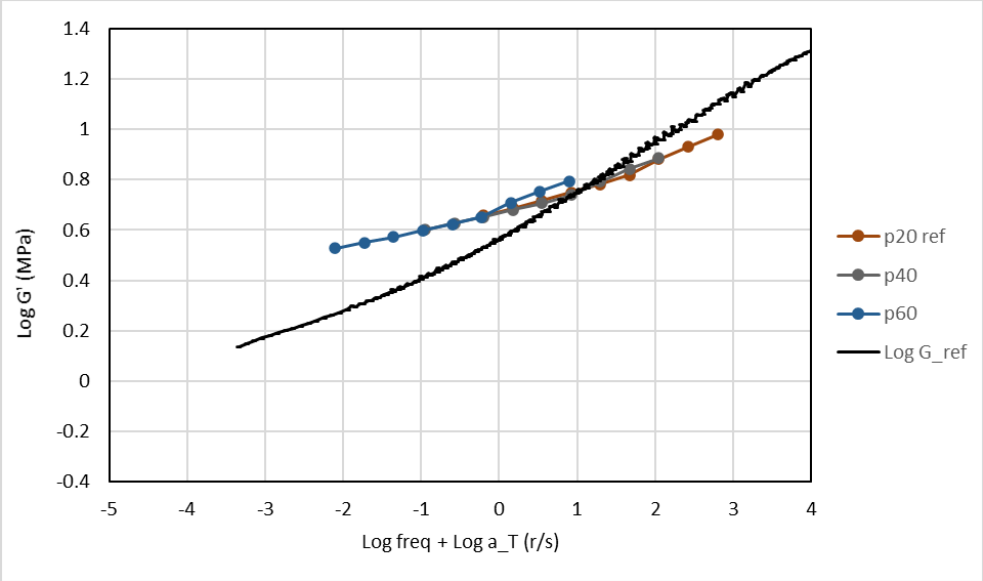

Figure 11: Master storage modulus curve for A50 neoprene compared to master curve for filled HTPB (Log G_ref).

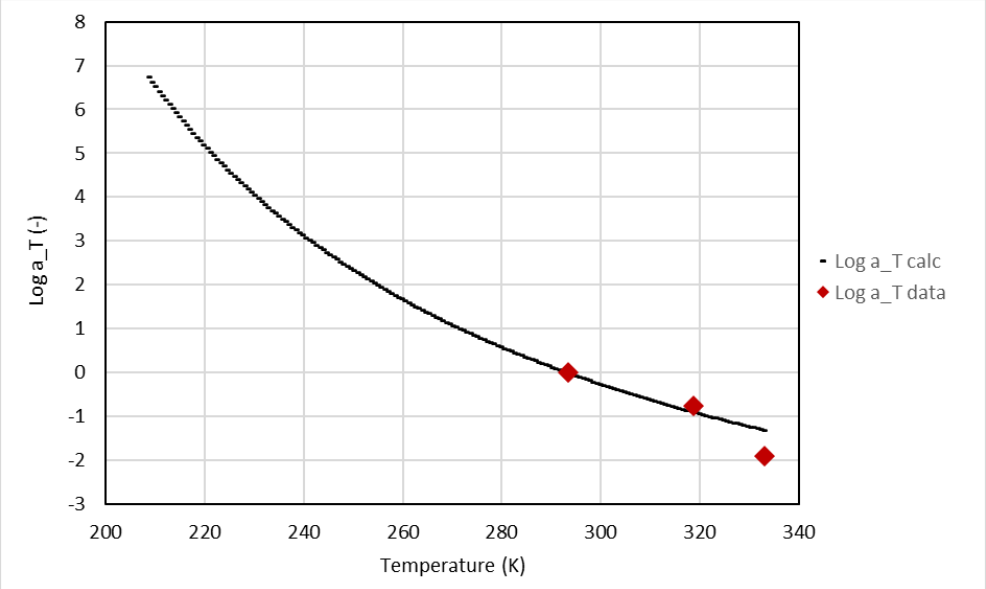

Figure 12: WLF shift factors for A50 neoprene compared to shift factors for filled HTPB (Log a_T calc).

6.3 Neoprene A60 Results

The master curve in the frequency domain for the neoprene with a Shore A60 is shown in Figure 13Figure 9. The shift factors are shown in Figure 14Figure 11. The filled-HTPB master curve and Williams-Landel-Ferry (WLF) curve are provided for reference.

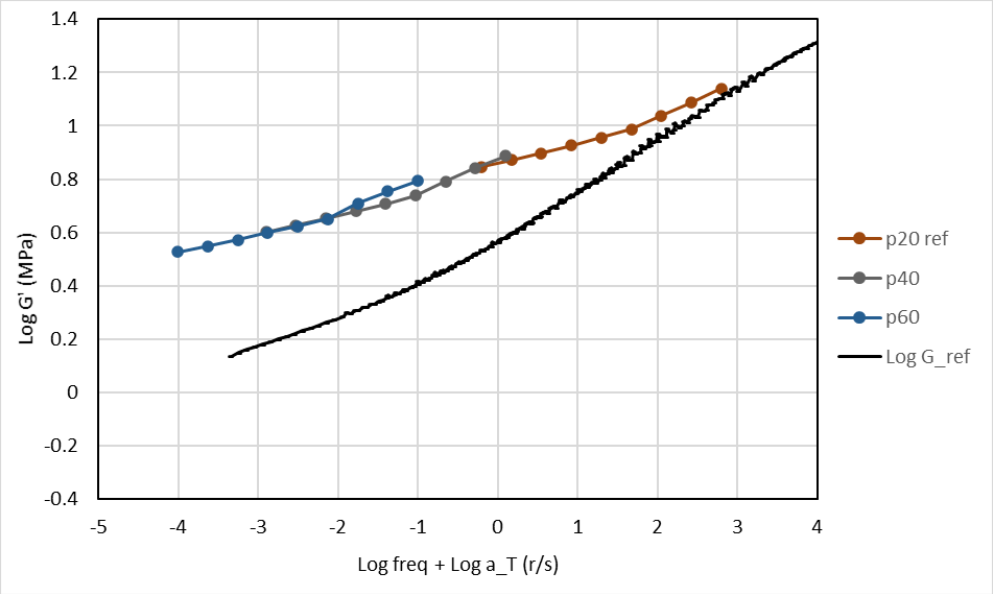

Figure 13: Master storage modulus curve for A60 neoprene compared to master curve for filled HTPB (Log G_ref).

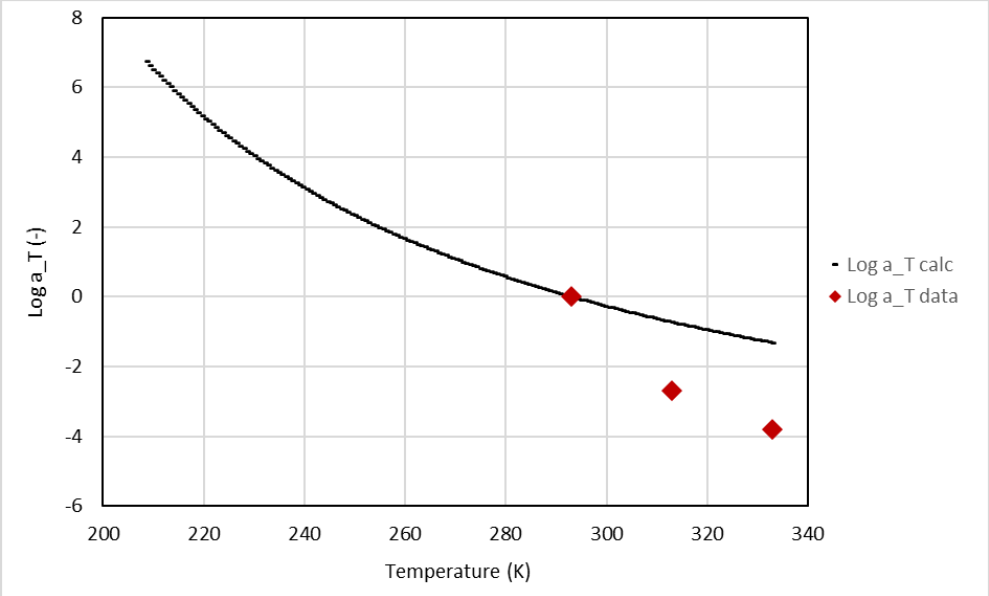

Figure 14: WLF shift factors for A60 neoprene compared to shift factors for filled HTPB (Log a_T calc).

6.4 Neoprene A70 Results

The master curve in the frequency domain for the neoprene with a Shore A70 is shown in Figure 15Figure 9. The shift factors are shown in Figure 16Figure 11. The filled-HTPB master curve and Williams-Landel-Ferry (WLF) curve are provided for reference.

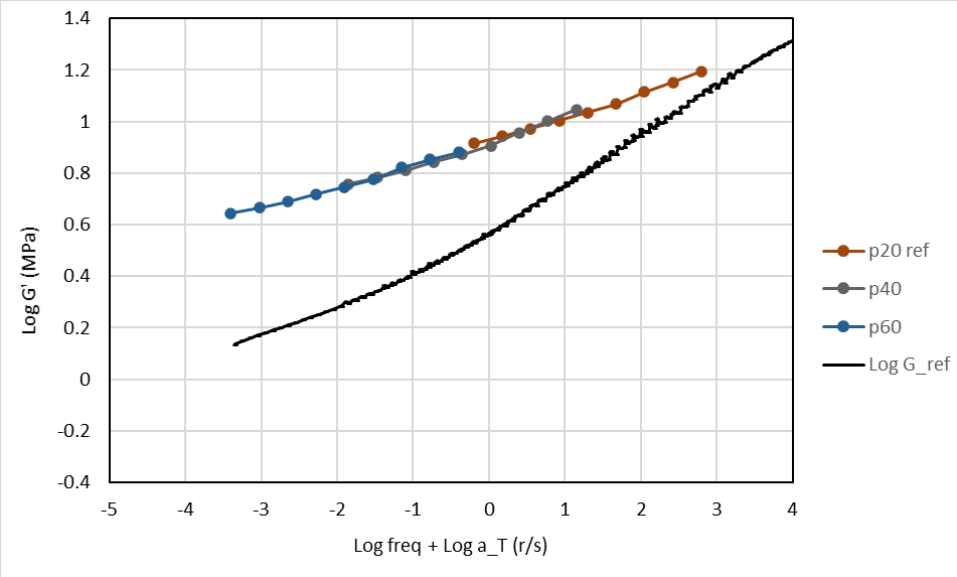

Figure 15: Master storage modulus curve for A70 neoprene compared to master curve for filled HTPB (Log G_ref).

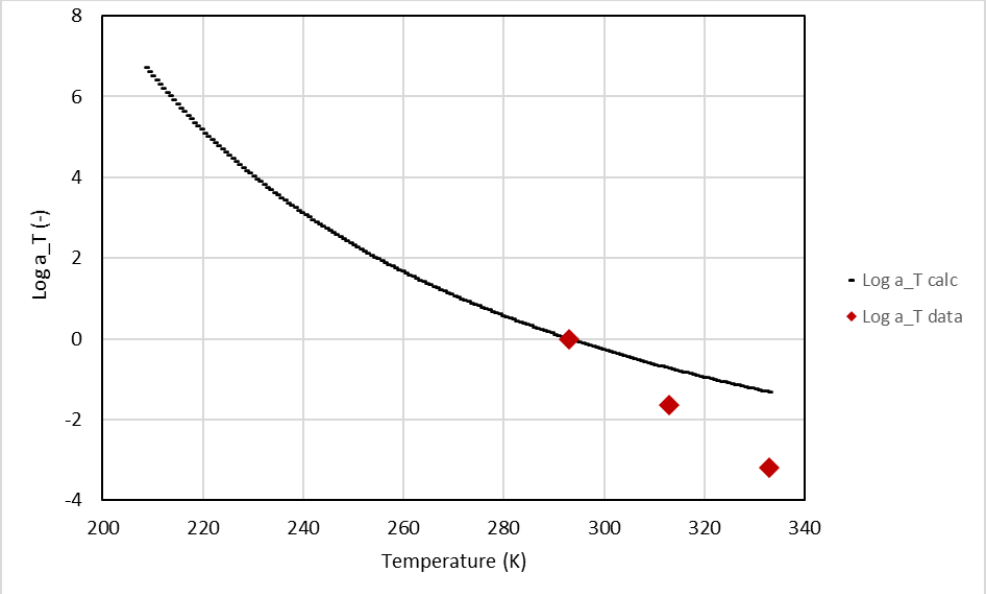

Figure 16: WLF shift factors for A70 neoprene compared to shift factors for filled HTPB (Log a_T calc).

6.5 Discussion

Figure 17 provides a composite view of the neoprene storage modulus data in the frequency domain relative to the filled-HTPB data. The shift factors are shown in Figure 18.

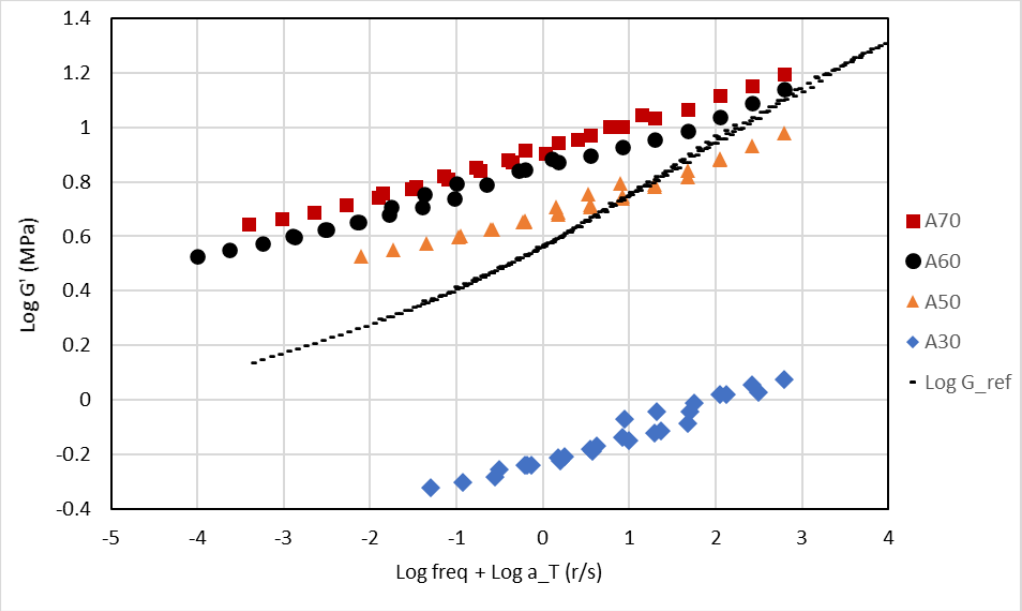

Figure 17: Composite master storage modulus curve for neoprene compared to master curve for filled HTPB (Log G_ref).

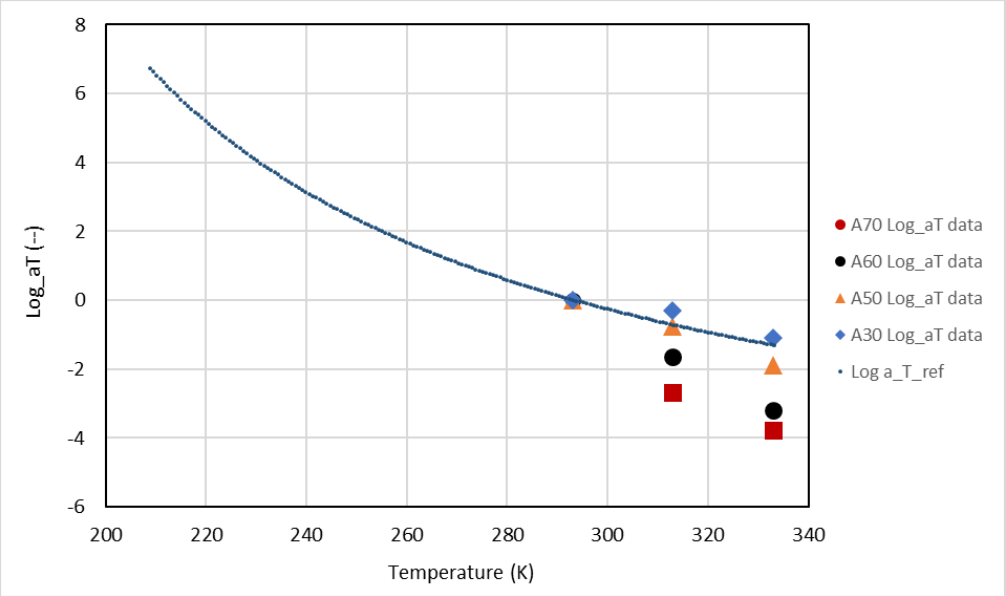

Figure 18: Composite WLF shift factors for neoprene compared to shift factors for filled HTPB (Log a_T ref).

From a qualitative point of view, it can be seen that there is a substantial increase in storage modulus between the Shore A30 and the Shore A50 neoprene. The changes in storage moduli are not linear with the hardness and appear to decrease with increasing hardness. The storage modulus increases smoothly with increasing frequency as expected. The shift factors increase in magnitude with increasing hardness.

The results obtained for the neoprene in this Section using the test method and values as described in Section 5 appear to be self-consistent. It was concluded that the dynamic micro-indentation method and test values are suitable for characterizing the storage modulus of the inert propellant polymer.

7. ACCELERATED AGED MATERIAL MEASUREMENTS

The accelerated aged inert propellant slabs were withdrawn from the 140 F oven at the time intervals listed in Section 4, Table 3. Samples were taken from a location at least 1 in. (25 mm) from the edge of the slab. Each 0.5 in. thick slab was cut through the thickness and perpendicular to the slab edge with a straight-edge razor blade to produce a 0.5 in. W x 0.8 in. L x 0.08 in. T (12 mm W x 20 mm L x 2 mm T) sample. The sample was installed in the micro-indenter sample holder and conditioned for a minimum of 30 min. to allow it to reach thermal equilibrium. The temperature controller has a control tolerance of +/-1 C. The samples were tested at 20 C, 40 C and 60 C. A frequency sweep between 1 Hz and 100 Hz in 7 equal increments in log frequency space was carried out over a minimum of seven (7) test locations on the sample. Each temperature created a complex modulus dataset as a function of frequency. The test values used in the test method are shown in Table 7.

Table 7. Values Used in Test Method for Inert Propellant

Parameter	**Value**
Flat punch diameter (µm)	53.1
Phase change for contact (deg)	8
Surface pre-compression (µm)	1
Dynamic force (µN)	50
Maximum dynamic displacement (nm)	200
Creep determination time (s)	30
Creep tolerance (nm/s)	0.5
Waves to average dynamics (-)	5

The data in each dataset was reduced by first filtering out the two (2) highest and two (2) lowest storage modulus data points corresponding to four (4) test locations at each frequency and then averaging three (3) remaining data points corresponding to three (3) test locations to calculate the mean and standard deviation of the storage modulus, loss modulus and loss factor. This method of filtering the results was effective in controlling the variability caused by the possible presence of the hard particles around and underneath the test locations. Though not shown here, it was observed that the mean values obtained for 7 test locations (0 filtering of data points) and 5 test locations (filtering of highest and lowest data points) converged to the mean value for 3 test locations (filtering of 2 highest and 2 lowest data points).

The mean values of the storage moduli are presented here. To provide a reference point for visual comparison, unpublished storage modulus data for a filled-HTPB is shown along with the measured storage modulus results. For additional information about the filled-HTPB data, see Annex C.

Figure 19 shows a photograph of the inert propellant surface with a 1 mm (1000 µm) wide screwdriver blade for reference. The flat punch indenter has a diameter of 53.1 µm. As seen in Figure 19 the ammonium sulfate particles are quite large compared to the indenter diameter. The test locations were judiciously chosen so that there was at least 150 µm separation between the nearest particle and the indenter.

Figure 19: Inert propellant with 1000 µm wide screwdriver blade. Flat punch indenter used for dynamic micro-indentation measures 53.1 µm dia.

7.1 Inert 0 Day Aged Results

The master curve in the frequency domain for the 0 day accelerated aged inert propellant is shown in Figure 20Figure 9. The shift factors are shown in Figure 21Figure 11. The filled-HTPB master curve and its Williams-Landel-Ferry (WLF) curve are provided for reference.

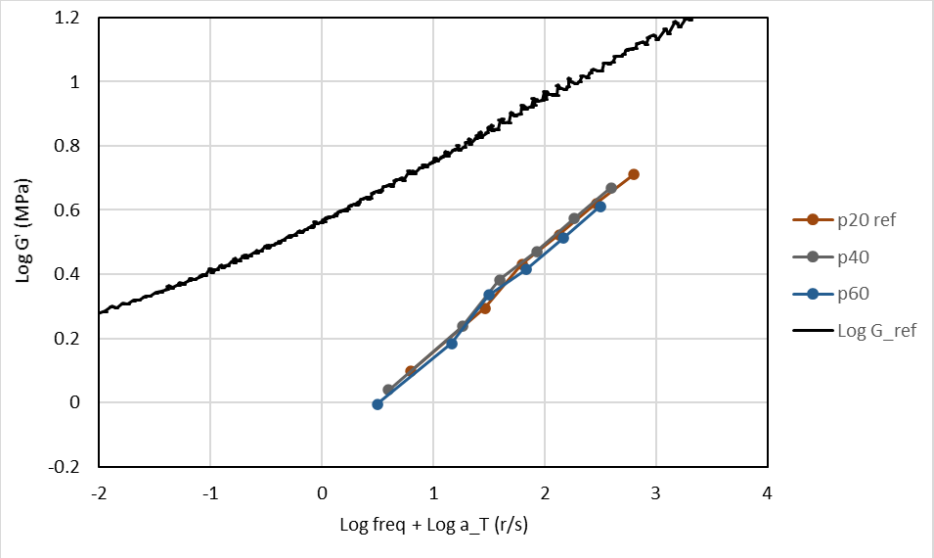

Figure 20: Master storage modulus curve for 0 day aged inert propellant compared to master curve for filled HTPB (Log G_ref).

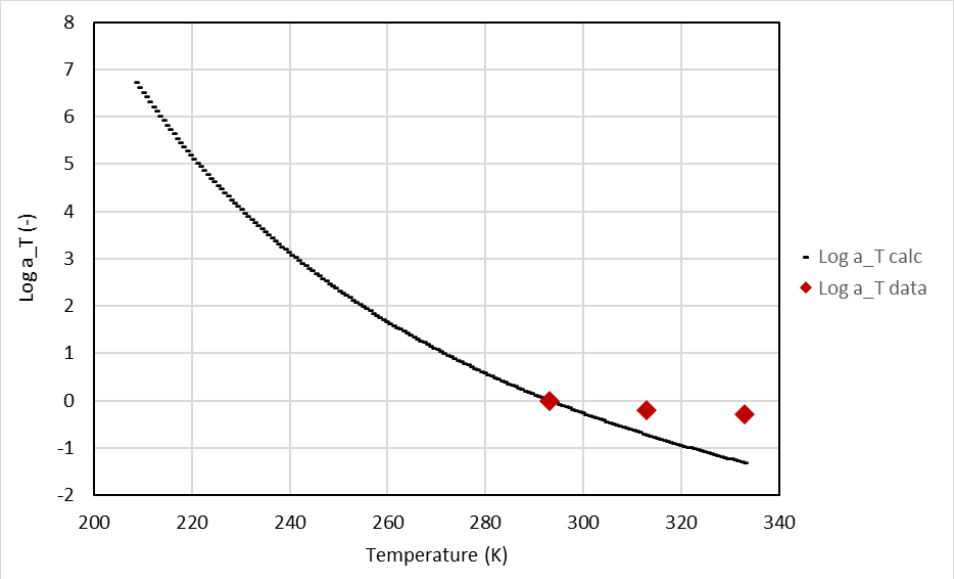

Figure 21: WLF shift factors for 0 day aged inert propellant compared to shift factors for filled HTPB (Log a_T calc).

7.2 Inert 7 Day Aged Results

The master curve in the frequency domain for the 7 day accelerated aged inert propellant is shown in Figure 22Figure 9. The shift factors are shown in Figure 23Figure 11. The filled-HTPB master curve and its Williams-Landel-Ferry (WLF) curve are provided for reference.

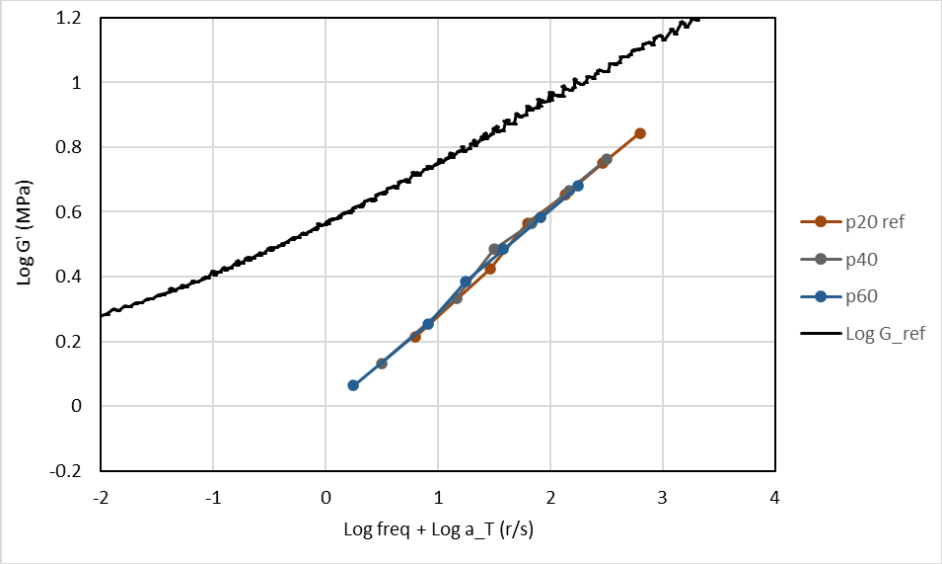

Figure 22: Master storage modulus curve for 7 day aged inert propellant compared to master curve for filled HTPB (Log G_ref).

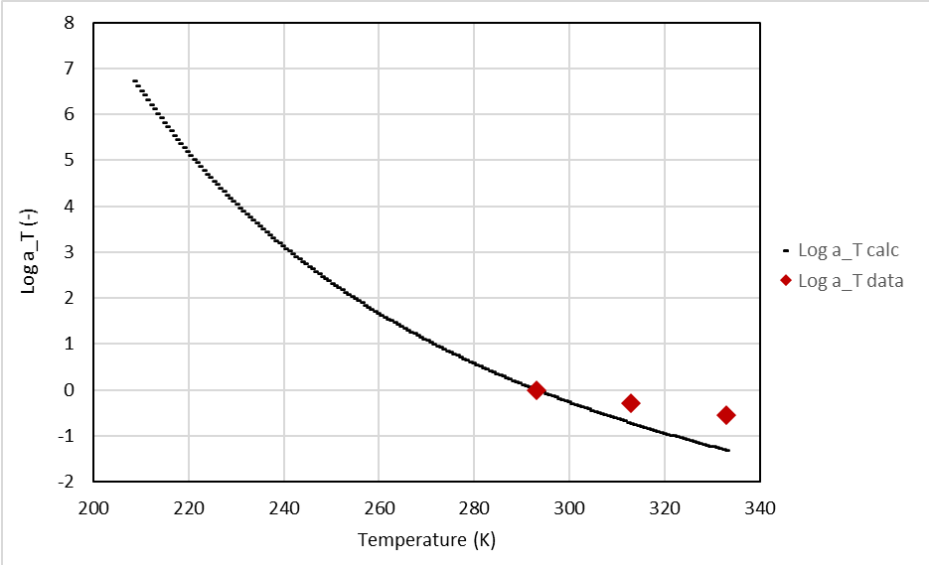

Figure 23: WLF shift factors for 7 day aged inert propellant compared to shift factors for filled HTPB (Log a_T calc).

7.3 Inert 15 Day Aged Results

The master curve in the frequency domain for the 15 day accelerated aged inert propellant is shown in Figure 24Figure 9. The shift factors are shown in Figure 25Figure 11. The filled-HTPB master curve and its Williams-Landel-Ferry (WLF) curve are provided for reference.

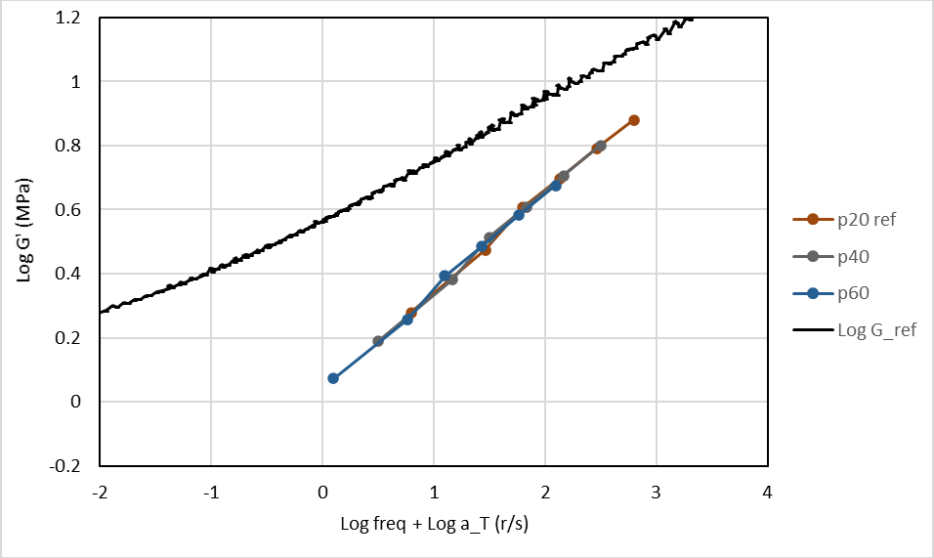

Figure 24: Master storage modulus curve for 15 day aged inert propellant compared to master curve for filled HTPB (Log G_ref).

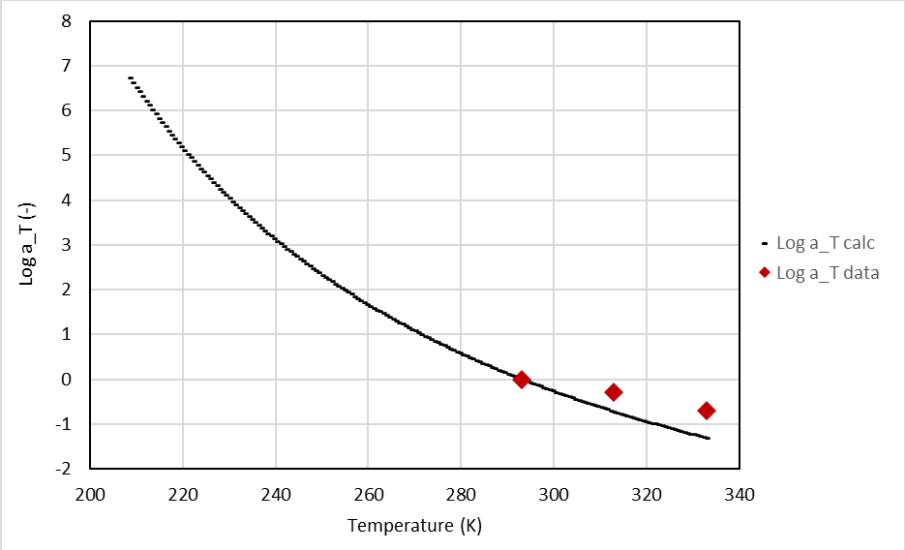

Figure 25: WLF shift factors for 15 day aged inert propellant compared to shift factors for filled HTPB (Log a_T calc).

7.4 Inert 20 Day Aged Results

The master curve in the frequency domain for the 20 day accelerated aged inert propellant is shown in Figure 26Figure 9. The shift factors are shown in Figure 27Figure 11. The filled-HTPB master curve and its Williams-Landel-Ferry (WLF) curve are provided for reference.

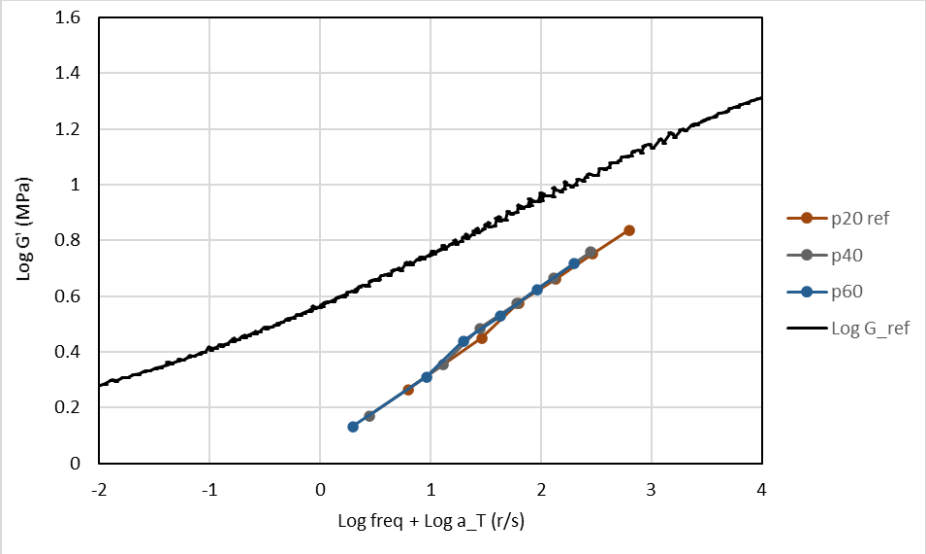

Figure 26: Master storage modulus curve for 20 day aged inert propellant compared to master curve for filled HTPB (Log G_ref).

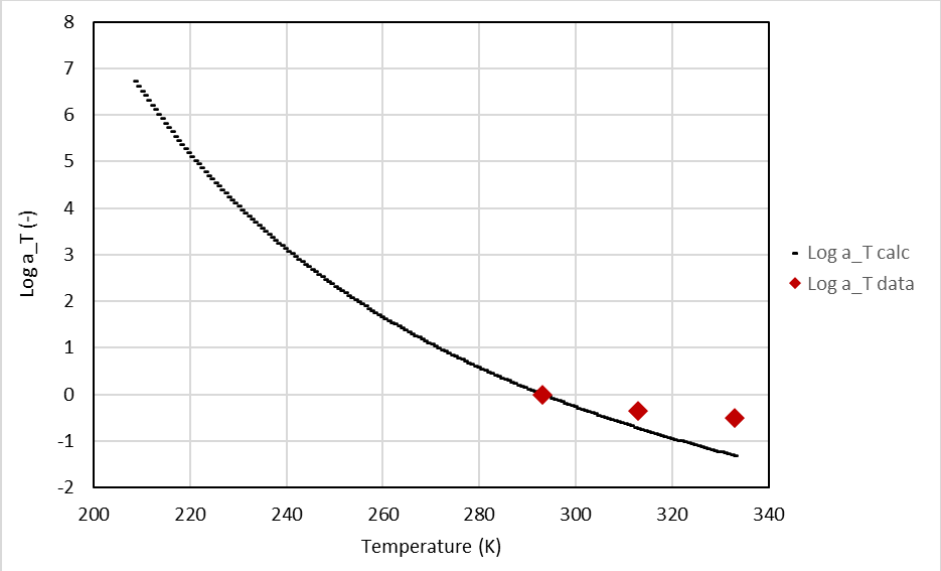

Figure 27: WLF shift factors for 20 day aged inert propellant compared to shift factors for filled HTPB (Log a_T calc).

7.5 Inert 40 Day Aged Results

The master curve in the frequency domain for the 40 day accelerated aged inert propellant is shown in Figure 28Figure 9. The shift factors are shown in Figure 29Figure 11. The filled-HTPB master curve and its Williams-Landel-Ferry (WLF) curve are provided for reference.

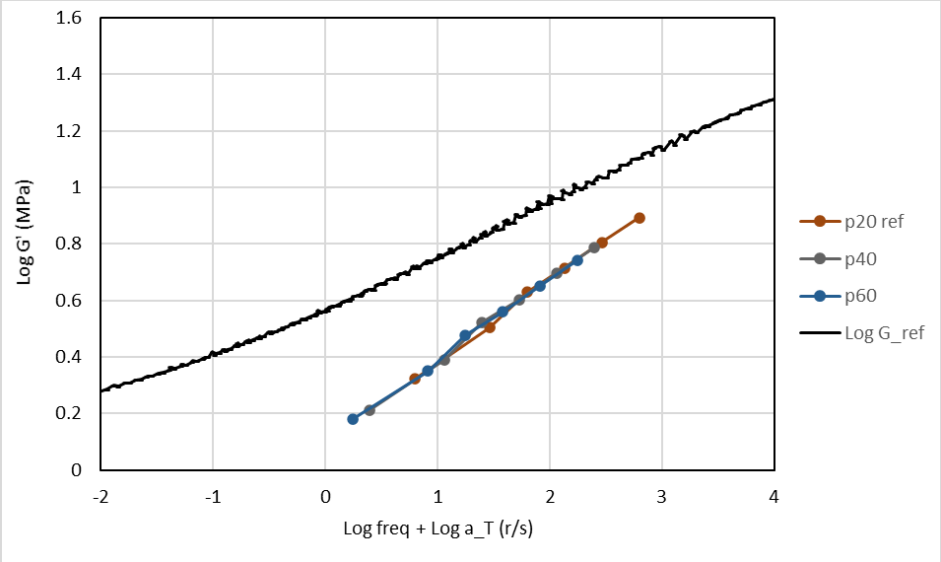

Figure 28: Master storage modulus curve for 40 day aged inert propellant compared to master curve for filled HTPB (Log G_ref).

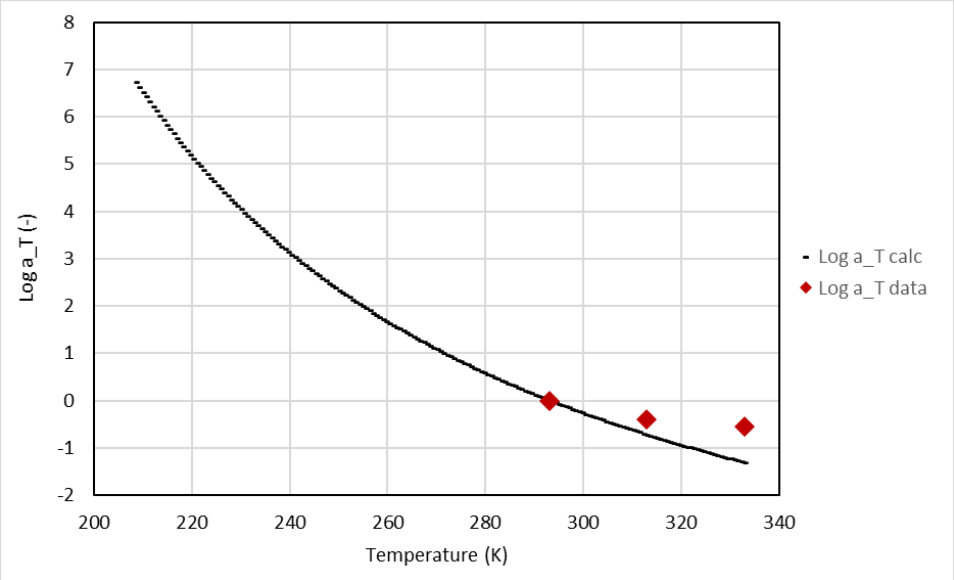

Figure 29: WLF shift factors for 40 day aged inert propellant compared to shift factors for filled HTPB (Log a_T calc).

7.6 Inert 60 Day Aged Results

The master curve in the frequency domain for the 60 day accelerated aged inert propellant is shown in Figure 30Figure 9. The shift factors are shown in Figure 31Figure 11. The filled-HTPB master curve and its Williams-Landel-Ferry (WLF) curve are provided for reference.

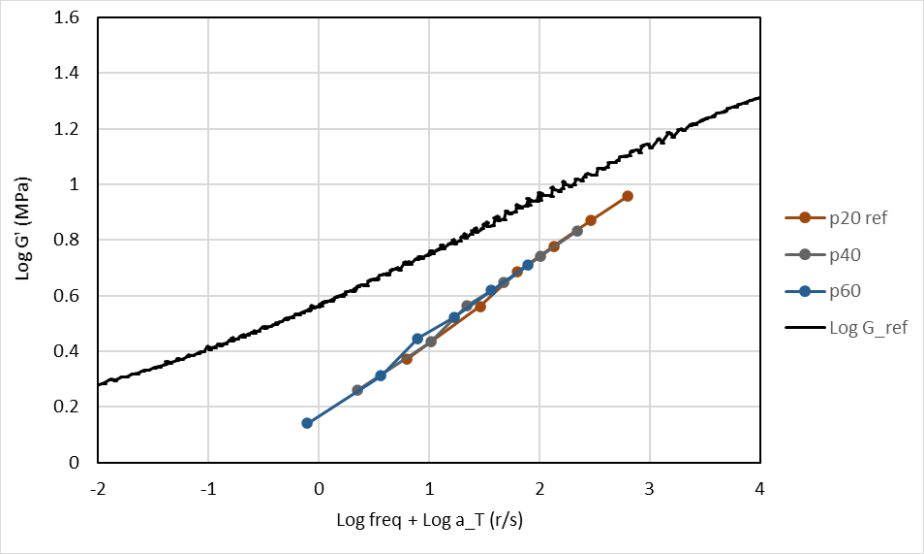

Figure 30: Master storage modulus curve for 60 day aged inert propellant compared to master curve for filled HTPB (Log G_ref).

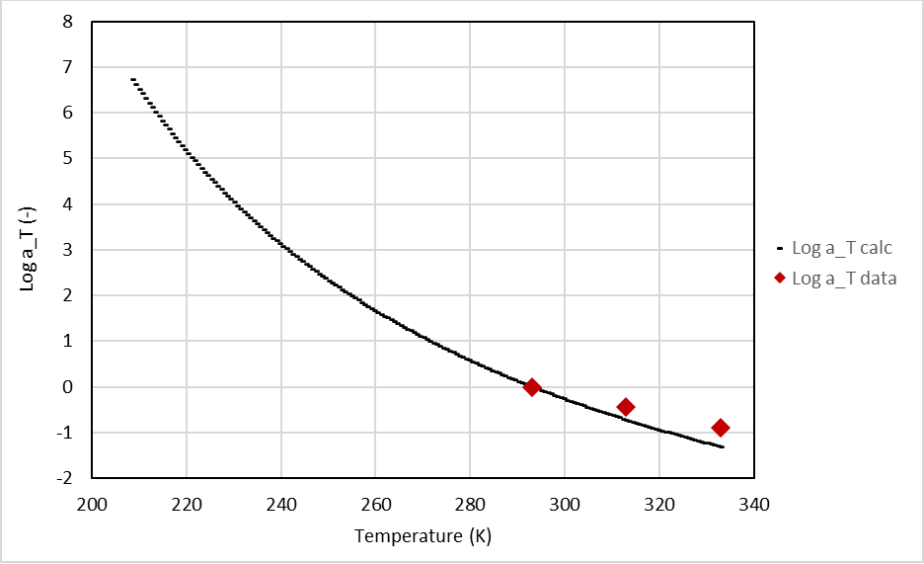

Figure 31: WLF shift factors for 60 day aged inert propellant compared to shift factors for filled HTPB (Log a_T calc).

7.7 Inert 80 Day Aged Results

The master curve in the frequency domain for the 80 day accelerated aged inert propellant is shown in Figure 32Figure 9. The shift factors are shown in Figure 33Figure 11. The filled-HTPB master curve and its Williams-Landel-Ferry (WLF) curve are provided for reference.

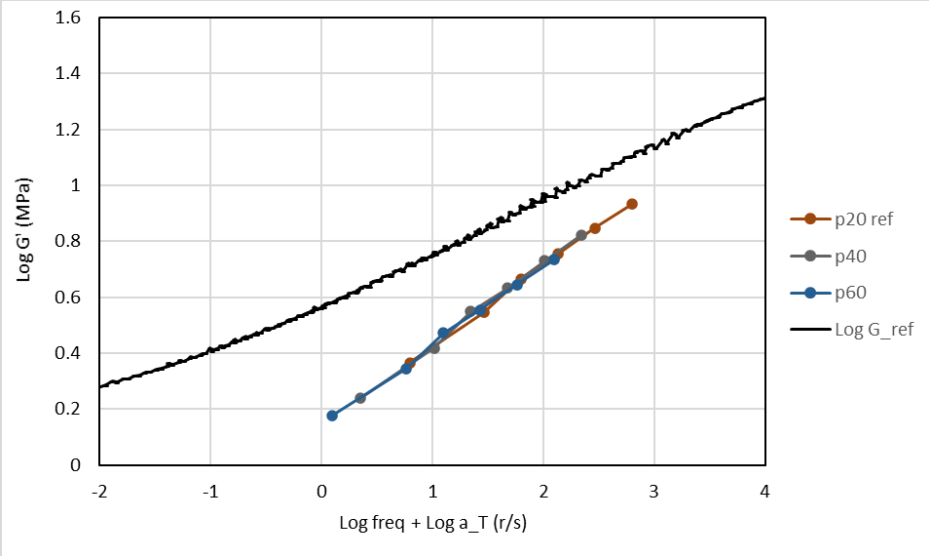

Figure 32: Master storage modulus curve for 80 day aged inert propellant compared to master curve for filled HTPB (Log G_ref).

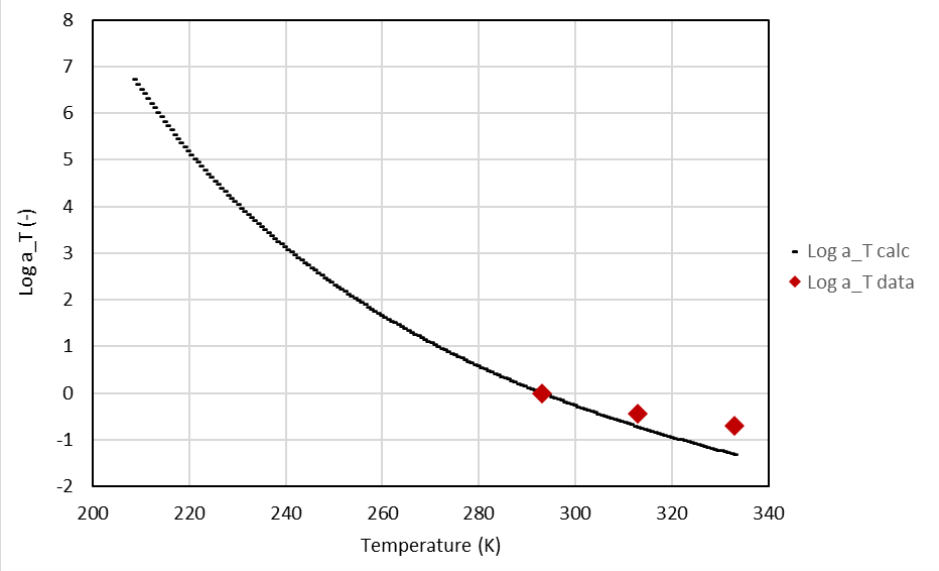

Figure 33: WLF shift factors for 80 day aged inert propellant compared to shift factors for filled HTPB (Log a_T calc).

7.8 Inert 100 Day Aged Results

The master curve in the frequency domain for the 100 day accelerated aged inert propellant is shown in Figure 34Figure 9. The shift factors are shown in Figure 35Figure 11. The filled-HTPB master curve and its Williams-Landel-Ferry (WLF) curve are provided for reference.

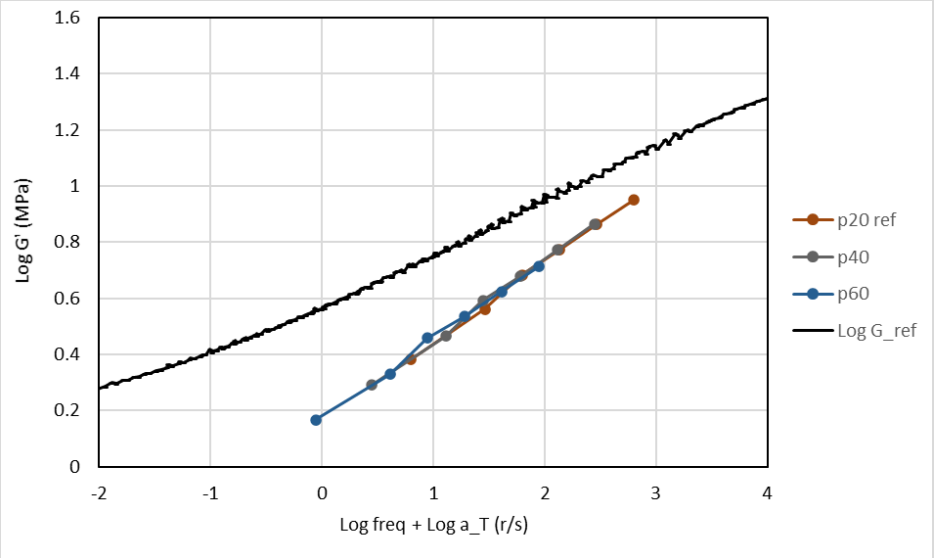

Figure 34: Master storage modulus curve for 100 day aged inert propellant compared to master curve for filled HTPB (Log G_ref).

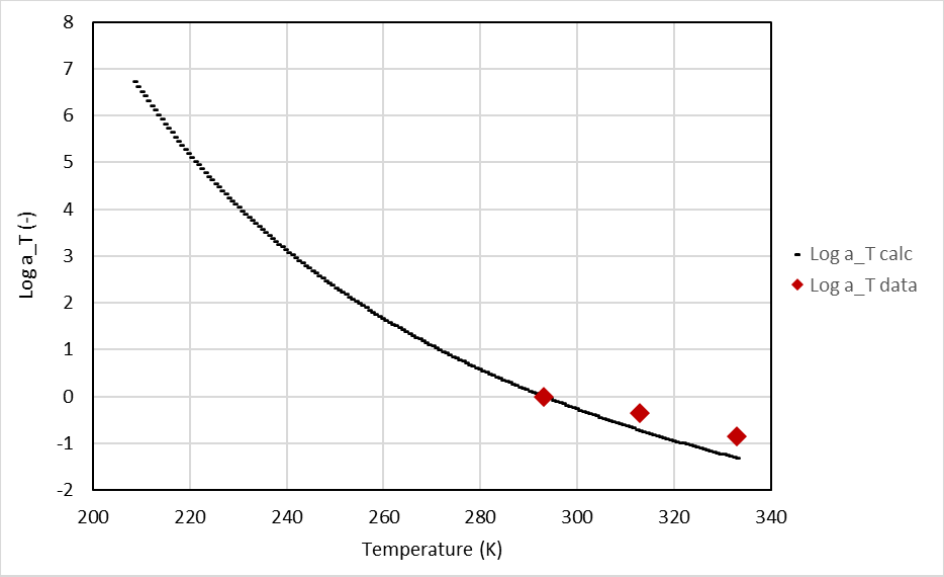

Figure 35: WLF shift factors for 100 day aged inert propellant compared to shift factors for filled HTPB (Log a_T calc).

7.9 Inert 120 Day Aged Results

The master curve in the frequency domain for the 120 day accelerated aged inert propellant is shown in Figure 36Figure 9. The shift factors are shown in Figure 37Figure 11. The filled-HTPB master curve and its Williams-Landel-Ferry (WLF) curve are provided for reference.

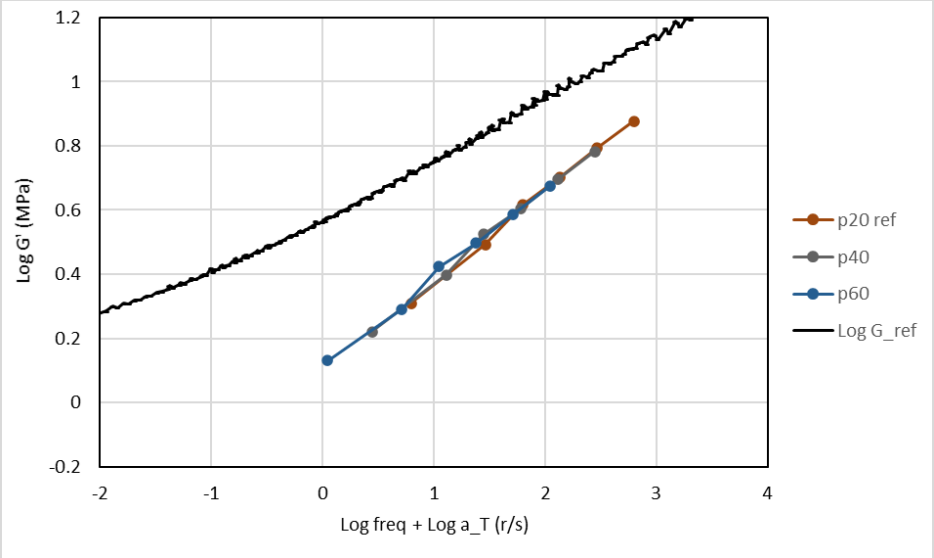

Figure 36: Master storage modulus curve for 120 day aged inert propellant compared to master curve for filled HTPB (Log G_ref).

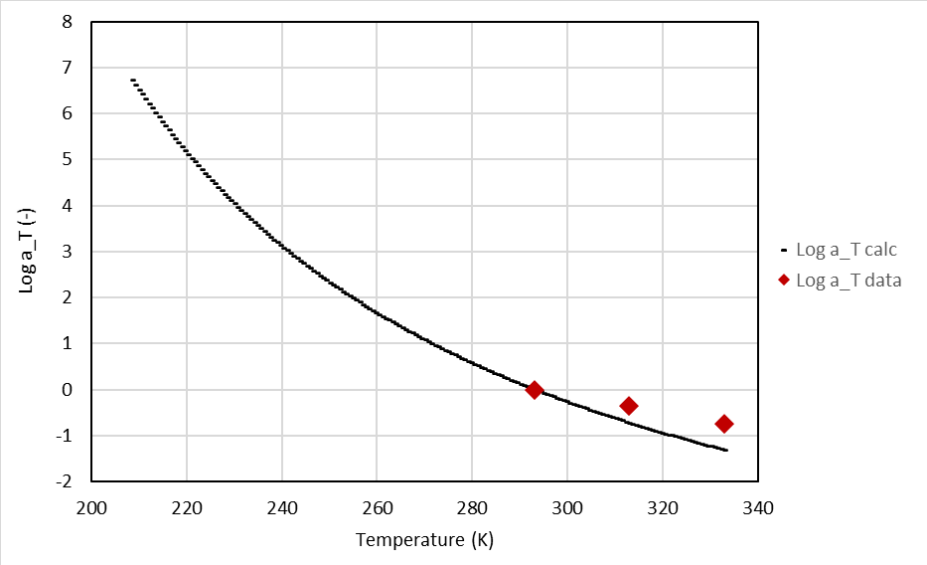

Figure 37: WLF shift factors for 120 day aged inert propellant compared to shift factors for filled HTPB (Log a_T calc).

7.10 Discussion

Figure 38 provides a composite view of the accelerated aged inert propellant storage modulus data in the frequency domain relative to the filled-HTPB data. The shift factors are shown in Figure 39. The results from a filled-HTPB propellant are shown for reference.

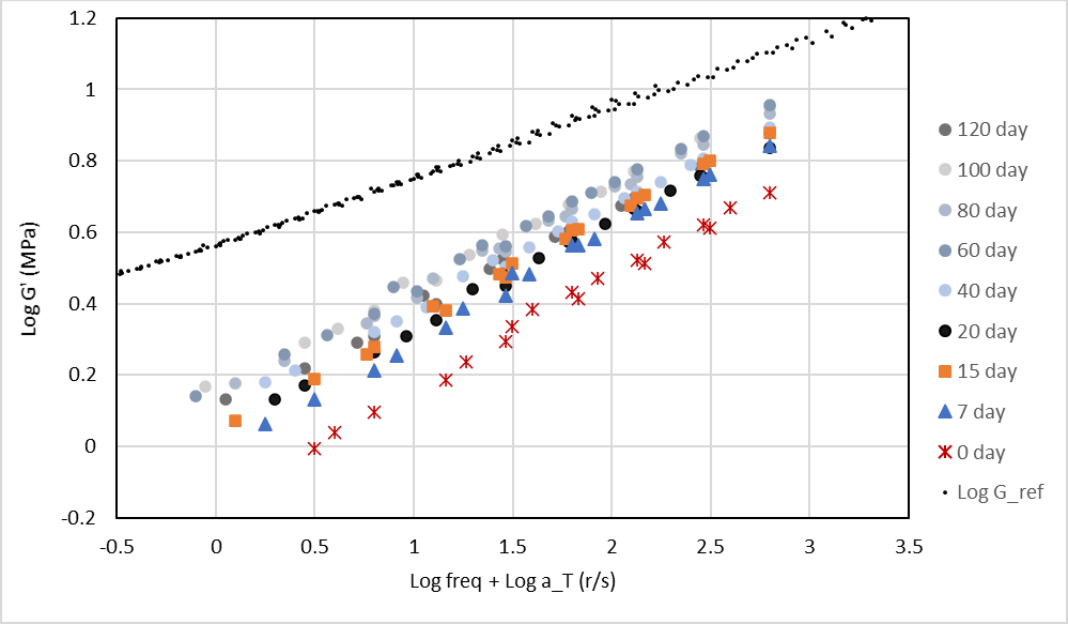

Figure 38: Composite master storage modulus curve for accelerated aged inert propellant compared to master curve for filled HTPB (Log G_ref).

The increase in stiffness of the inert propellant between the 0 day propellant and the 7 day propellant can be qualitatively seen in Figure 38. The 15 and 20 day propellants appear to have a slightly higher stiffness than the 7 day propellant. The 40 to 120 day propellants generally look stiffer than the 15 and 20 day propellants.

The WLF shift factors show a general trend where the longer aging times have larger shift factors. The magnitude of the shift factor differences is more observable with the hotter 60 C (333 K) data. It can be seen in the 15 and 20 day data points at 333 K that trend is not entirely consistent.

The increase in stiffness as a function of aging time was further analysed by using linear regression on the datasets to make the comparison more quantitative. Figure 40 presents the average and upper and lower 95% confidence limits from the regression analysis. Preliminary analyses, not provided here, showed that some of the datasets could be grouped together because the differences between them were small. As Figure 40 clearly reveals, there are statistical differences among the 0 day, 7 day, 15 to 20 day, 40 to 100 day and 120 day accelerated aging datasets. The inert propellant hardens from 0 to 100 days and then softens at 120 days of aging.

The results suggest that the increased stiffness up to 100 days may be attributed to increased crosslink density from oxidation in the inert propellant polymer. The decrease in stiffness may be attributed to decreased crosslink density from chain scission or hydrolysis [27].

It was concluded that the measured storage modulus data reflected the crosslink density state of the aged inert propellant polymer.

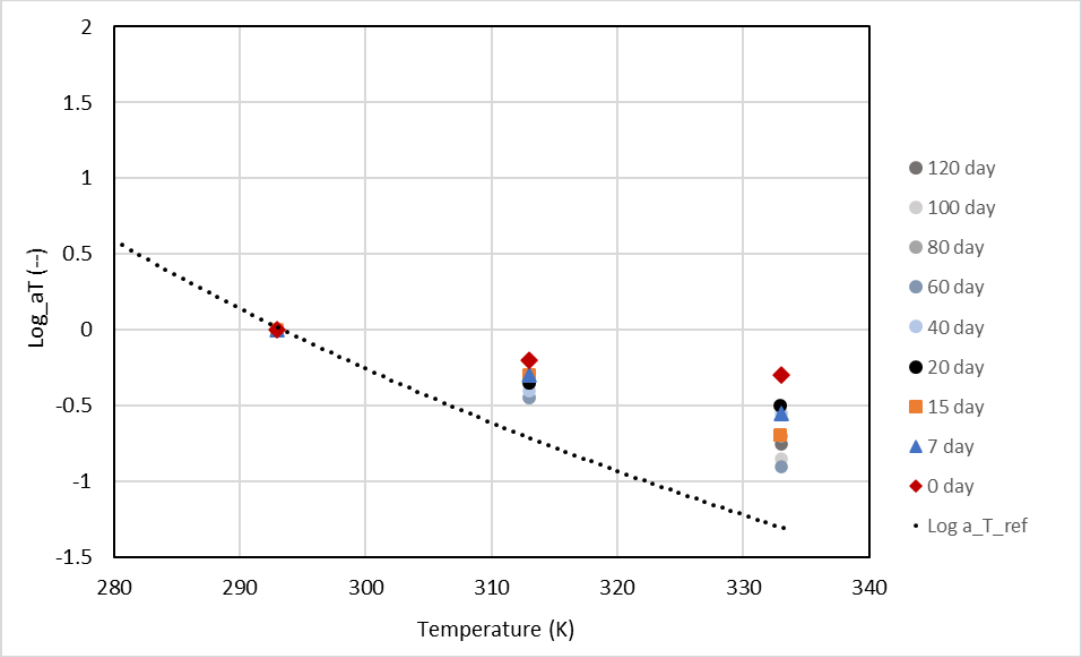

Figure 39: Composite WLF shift factors for accelerated aged inert propellant compared to shift factors for filled HTPB (Log a_T ref).

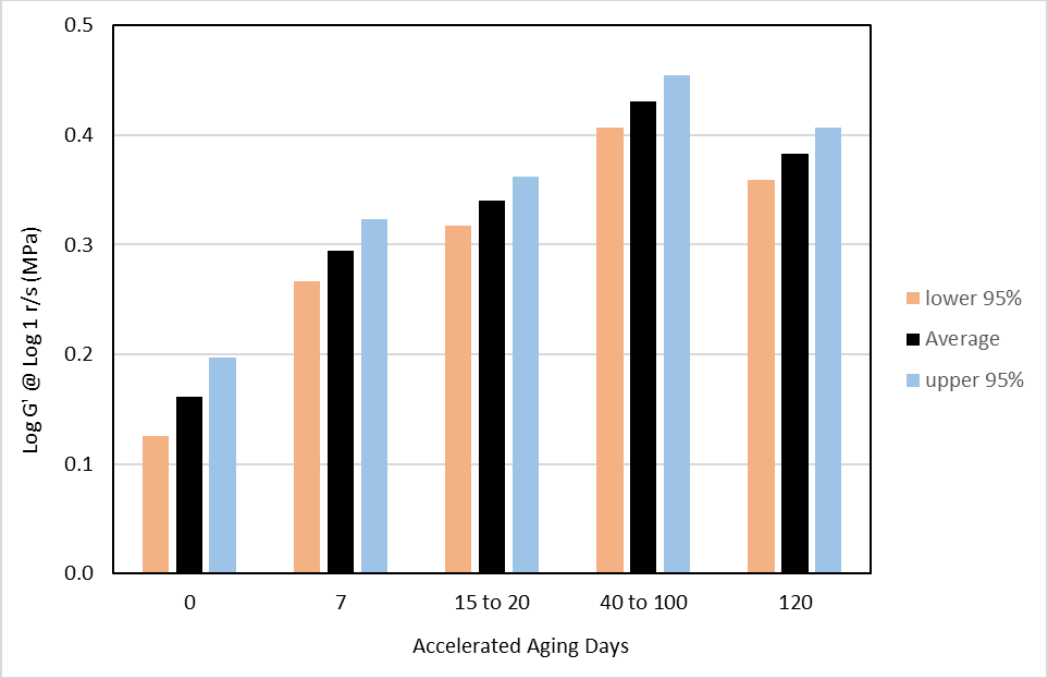

Figure 40: Increase in storage modulus at Log 1 r/s as a function of accelerated aging time. Average and percentile limits shown.

8. CROSSLINK DENSITY RESULTS

The theory relating the dynamic micro-indentation measurements to crosslink density was provided in Section 3. Recall the relationship given in eq. 18

$$\gamma = \frac{1}{R_c T}\left[\frac{E'}{2(1+\vartheta_p)}\right] \tag{18}$$

where γ is the crosslink density of the material under test (mole/m^3),
R_c is the universal gas constant (8.3143 m^3 Pa kg^{-1} K^{-1}),
T is the absolute temperature during test (K),
ϑ_p is the Poisson ratio of the material under test (0.495),
E′ is the storage modulus measured by the micro-indenter (Pa).

Figure 41 plots the measured storage moduli at 1 Hz for the three test temperatures 20 C, 40 C and 60 C. The lowest frequency data was used to be as close as possible to the equilibrium modulus conditions. Recall that the micro-indenter and specimen geometry means the instrument measures tensile storage modulus and not shear storage modulus. The error bars represent the standard deviation calculated from filtering the seven measurements down to three. Table 8 lists the numeric values corresponding to the bars in Figure 41. The color coding in the Table groups the aged results according to the statistically significant groupings discussed in Section 7.

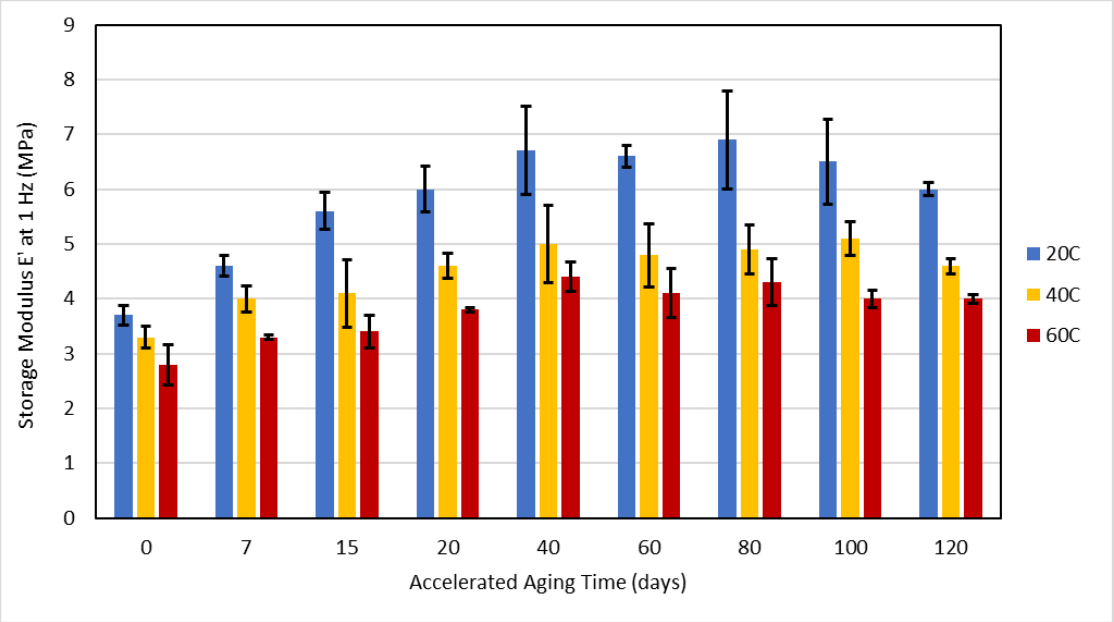

Figure 41: Tensile storage moduli measured at 1 Hz and 20 C, 40 C and 60 C as a function of accelerated aging time.

Table 8. Storage Moduli at 1 Hz for Aged Inert Propellant

Accel	**20C**			**40C**			**60C**		
Aged	E'@ 1 Hz	std dev	std dev	E'@ 1 Hz	std dev	std dev	E'@ 1 Hz	std dev	std dev
Day	(MPa)	(%)	(MPa)	(MPa)	(%)	(MPa)	(MPa)	(%)	(MPa)
0	3.7	5	0.2	3.3	6	0.2	2.8	13	0.4
7	4.6	4	0.2	4.0	6	0.2	3.3	1	0.0
15	5.6	6	0.3	4.1	15	0.6	3.4	9	0.3
20	6.0	7	0.4	4.6	5	0.2	3.8	1	0.0
40	6.7	12	0.8	5.0	14	0.7	4.4	6	0.3
60	6.6	3	0.2	4.8	12	0.6	4.1	11	0.5
80	6.9	13	0.9	4.9	9	0.4	4.3	10	0.4
100	6.5	12	0.8	5.1	6	0.3	4.0	4	0.2
120	6.0	2	0.1	4.6	3	0.1	4.0	2	0.1

When the increase in storage modulus is compared to the expected increase in modulus shown in Table 3, it is evident that the inert propellant in this study did not harden like the aged NGIS propellant. For example, the ratio of the micro-indenter 100 day-to-0 day storage modulus is only 1.8X while the NGIS measured ratio was 6.5X.

To investigate the cause of this disparity, Shore A tests were carried out on the accelerated aged slabs of inert propellant. The Shore A indenter was allowed to settle for 12 s before the reading was taken. Table 9 lists the NGIS-measured Shore A (from Table 2), the Micron-measured Shore A and the storage modulus measured by the micro-indenter.

Table 9. Comparison of Shore A and Storage Moduli for Aged Inert Propellant

Aging @ 140 F	**0 day**	**15 day**	**20 day**	**40 day**	**60 day**	**80 day**	**100 day**	**120 day**
NGIS Shore A	38		56		75		71	
Micron Shore A	57	63	66	65	67	69	70	69
Micron E' (MPa) @ 1 Hz	3.7	5.6	6.0	6.7	6.6	6.9	7.0	6.0

Comparing the NGIS Shore A with the Micron Shore A, it can be seen that the Micron 0 day Shore A is much higher than the NGIS Shore A at 0 day. The NGIS Shore A reached a plateau at 60 days while the Micron Shore A reached a lower plateau after 20 days and a higher plateau after 80 days. The Micron E′ storage modulus at 1 Hz tracked generally the trend seen in the Micron Shore A data.

Micron started testing the inert propellant samples at the beginning of Dec. 2020. The NGIS and Micron Shore A data indicate that the inert propellant aged, while stored at room temperature, at Micron Instruments until testing could be carried out. The Shore A measurements of 56 (NGIS, 20 day) and 57 (Micron, 0 day) suggest that accelerated aging at 140 F for 20 days is roughly equivalent to aging at room temperature for eight months.

Returning to eq. 18, when it is applied to the storage modulus results in Table 8, the crosslink density results shown in Table 10 are obtained.

Table 10. Calculated Crosslink Densities for Aged Inert Propellant

Accel	**20C**		**40C**		**60C**	
Aged	Xlink density	std dev	Xlink density	std dev	Xlink density	std dev
Day	(mol/m^3)	(mol/m^3)	(mol/m^3)	(mol/m^3)	(mol/m^3)	(mol/m^3)
0	508	25	453	27	384	50
7	632	25	549	33	453	5
15	769	46	563	84	467	42
20	824	58	632	32	522	5
40	920	110	686	96	604	36
60	906	27	659	79	563	62
80	947	123	673	61	590	59
100	892	107	700	42	549	22
120	824	16	632	19	549	11

The crosslink density is proportional to the storage modulus since the universal gas constant and Poisson's ratio are constant at each temperature. According to the results shown in Table 10, the crosslink density at 20 C at 0 day is 508 mol/m^3. After 7 days of accelerated aging, the crosslink density increases to 632 mol/m^3. The crosslink density increases to 769 to 824 mol/m^3 after 15 to 20 days of aging. From 40 to 100 days of aging, the crosslink density increases further to 892 to 947 mol/m^3. After 120 days of aging, the crosslink density decreases to 824 mol/m^3. The crosslink density decreases with increasing temperature as expected.

It is not possible to say with the present dataset whether the storage modulus-derived crosslink density estimates are representative of the true crosslink density of the inert propellant. To make a definitive statement, the crosslink density of the inert propellant would need to be measured using the traditional and generally accepted equilibrium swelling method [28].

Annex A shows that an alternative method of comparison was planned using a similar approach as [8]. However, with the project scope reduction requested by the sponsor, there was insufficient time and funds to carry out the proposed work.

9. SUMMARY

The measurement of storage modulus using the dynamic micro-indenter method to enable calculation of crosslink density was investigated. Indentation methods are more tolerant to surface imperfections and dimensional variability in the test specimen. As a result, there is less time and effort needed for specimen preparation when using this technique.

Northrop Grumman Innovation Systems (NGIS) developed, under contract, an inert solid propellant that would age under accelerated aging conditions over an approximate 120 day period at a controlled rate. NGIS carried out an abbreviated aging study on the inert propellant shipped to Micron Instruments to verify the aging behavior.

The dynamic micro-indenter method was verified by testing neoprene sheet stock with Shore A values between 30 and 70. The results showed that the dynamic micro-indentation method was suitable for characterizing the storage modulus of the inert propellant polymer.

Inert propellant slabs were stored in an oven set at 140 F and withdrawn at the prescribed time intervals. Each test specimen was tested at 20 C, 40 C and 60 C. The indenter frequency was swept between 1 Hz and 100 Hz in seven equal increments in log frequency space over a minimum of seven test locations on the specimen.

The increase in storage modulus as a function of aging time was analysed. It was observed that some of the aging datasets could be grouped together because the difference in storage modulus between them were small. Statistical analyses showed that there were storage modulus differences among the 0 day, 7 day, 15 to 20 day, 40 to 100 day and 120 day accelerated aging datasets. The inert propellant hardened from 0 to 100 days aging and then softened at 120 days of aging.

The crosslink density was calculated with the measured storage modulus data. The results showed the crosslink density at 20 C at 0 day aging was 508 mol/m^3. After 7 days of accelerated aging, the crosslink density increased to 632 mol/m^3. The crosslink density increased to 769 to 824 mol/m^3 after 15 to 20 days of aging. From 40 to 100 days of aging, the crosslink density increased further to 892 to 947 mol/m^3. The crosslink density decreased to 824 mol/m^3 after 120 days of aging. The crosslink density decreased with increasing temperature as expected.

10. FUTURE WORK

The descoped effort left several activities that merit further effort.

The delay between the reception of the NGIS inert propellant and the start of dynamic micro-indentation at Micron Instruments was too long. The propellant aged a significant amount at room temperature. To support future work, a new batch of NGIS inert propellant with the same formulation would be required. Micron Instruments would start its accelerated aging schedule and sample tests shortly after the reception of the inert propellant.

To definitively show that the dynamic micro-indentation method is able to measure the crosslink density based on equilibrium storage modulus, a parallel characterization effort based on equilibrium swelling is recommended.

A companion comparison between the dynamic micro-indentation method and the traditional dynamic mechanical analysis method over a frequency range of 0.1 Hz to 100 Hz and temperature range of −60 C and +60 C would show if there is an equivalence between the two test methods. If an equivalence can be shown, the dynamic micro-indentation method would be a simpler, lower cost method to produce a master curve and the associated Prony-series and WLF shift factors for viscoelastic stress analyses.

The dynamic micro-indentation method is able to determine crosslink density through the measurement of storage modulus. Investigation into the miniaturization of the micro-indenter actuator to manufacture an in-situ crosslink density measurement sensor is recommended.

11. REFERENCES

[1] Fillerup, J.M., Wong, F.C., (2020), “Development of a Normal Shear Stress and Temperature (NSST) Sensor for Solid Rocket Motor Health Monitoring – Finite Element Analysis and Data Reduction”, Micron Instruments, Micron CR 2020-001, February 2020.

[2] Wong, F.C., Fillerup, J.M., (2020), “Development of a Normal Shear Stress and Temperature (NSST) Sensor Calibration Rig - Design and Validation”, Micron Instruments, Micron CR 2020-002, August 2020.

[3] Christiansen, AG, Layton, LH, Carpenter, RL, (1981), “HTPB Propellant Aging”, J. Spacecraft, 18 (3), 211-215.

[4] Judge, MD, (2003), “An Investigation of Composite Propellant Accelerated Ageing Mechanisms and Kinetics”, Propellants, Explosives, Pyrotechnics, 28 (3), 114-119.

[5] Ozupek, S, (1997), “Constitutive Equations for Solid Propellants”, Doctoral dissertation, U of Texas A&M.

[6] Martin, DL, (1970), “Crosslink Density Determinations for Polymeric Materials”, US Army Missile Command, Report RK-TR-70-6.

[7] Mujtaba, A, Keller, M., Ilisch, S., Radusch, HJ, Turn-Albrecht, T., Saalwachter, K, Beiner, M., (2012), “Mechanical Properties and Cross-Link Density of Styrene-Butadiene Model Composites Containing Fillers with Bimodal Particle Size Distribution”, Macromolecules, 45, 6504-6515.

[8] El-Sabbagh, S.H. et al., “Detection of Crosslink Density by Different Methods for Natural Rubber Blended with SBR and NBR”, Egypt. J. Solids, Vol. 30, 2007, pp. 157-174.

[9] Tan, S. et al., “Curing and Mechanical Properties of Nitrile and Natural Rubber Blends” J. Elastomer and Plast., Vol. 33, 2001, pp. 251-262.

[10] Treloar, L.R.G., "The Physics of Rubber Elasticity", 3rd., Oxford Univ. Press (1975).

[11] Jiang, H., et al., “Rheology of highly swollen chitosan/polyacrylate hydrogels”, Polymer, Vol. 40, 1999, pp. 4593-4602.

[12] TA Instruments, http://www.tainstruments.com/q800/#ffs-tabbed-11, accessed 25 Sep. 2017.

[13] Czerner, M., et al., “Determination of Elastic Modulus of Gelatin Gels by Indentation Experiments”, Procedia Mat. Sci., Vol. 8, 2015, pp. 287-296.

[14] Bles, G., et al., “Instrumented micro-hardness measurements used to identify the local visco-hyper-elastic parameters of Polyurethane elastomers", Constitutive Models for Rubber VIII - Gil-Negrete & Alonso (eds), 2013, pp. 177-182.

[15] Lin, D.C., “Spherical indentation of soft matter beyond the Hertzian regime: numerical and experimental validation of hyperelastic models”, Biomech Model Mechanobiol, Vol. 8, 2009, pp. 345-358.

[16] Herbert, E.G., Oliver, W.C., and Pharr, G.M., “Nanoindentation and the dynamic characterization of viscoelastic solids”, J. Phys. D: Appl. Phys. 41, 074021 (2008).

[17] Herbert, E.G., Oliver, W.C., Lumsdaine, A., Pharr, G.M., “Measuring the constitutive behavior of viscoelastic solids in the time and frequency domain using flat punch nanoindentation”, J. Mat. Res., Vol. 24, No. 3, 2009, pp. 626-637.

[18] Guglielmi, P.O., Herbert, E.G., Tartivel, L.; Behl, M., Lendlein, A., Huber, N., Lilleodden, E.T., “Mechanical characterization of oligo(ethylene glycol)-based hydrogels by dynamic nanoindentation experiments”, J Mech Behav Biomed Mater, Vol. 46, 2015, pp. 1-10.

[19] Standardized Nanoindentation: ISO 14577, http://nanomechanicsinc.com/wp/wp-content/uploads/2015/12/App-Note-Interactive.pdf, accessed 15 Jan. 2021.

[20] Sneddon, I.N., “The relaxation between load and penetration in the axisymmetric Boussinesq problem for a punch of arbitrary profile”, Int. J. Engng. Sci., Vol. 3, 1965, pp. 45-57.

[21] Oliver, W.C., Pharr, G.M., “An improved technique for determining hardness and elastic modulus using load and displacement sensing indentation experiments”, J. Mater. Res., 1992, Vol. 7, 1564-1583.

[22] Oliver, W.C., Pharr, G.M., “Measurements of hardness and elastic modulus by instrumented indentation: Advances in understanding and refinements to methodology”, J. Mat. Res., Vol. 19, No. 1, 2004, pp. 3-20.

[23] Pelletier, C.G.N., “Mechanical characterization of glassy polymers using instrumented indentation”, PhD thesis, Eindhoven University of Technology, 2008.

[24] http://nanomechanicsinc.com/imicro/, accessed 20 January 2021.

[25] Hay, J., Nanomechanics personal communication, 23 October 2020.

[26] http://www.warco.com/sheet-rubber/neoprene/commercial-neoprene-style-10/, accessed 21 January 2021.

[27] Adel, W.M., Liang, G., "Service life prediction of AP/Al/HTPB solid rocket propellant with consideration of softening aging behavior", Chinese J. Aero., Vol. 32, No. 2, 2019, pp. 361-368.

[28] Sekkar, V., Raunija, T.S.K., "Hydroxyl-terminated polybutadiene-based polyurethane networks as solid propellant binder-State of the art", J. Prop. Power, Vol. 31, No. 1, 2015, pp. 16-35.

ANNEX A – STATEMENT OF WORK FOR INERT PROPELLANT DEVELOPMENT

This Annex contains the two statements of work provided to Northrop Grumman Innovation Systems (NGIS) for the development of the inert propellant used in the dynamic micro-indentation study, a set of companion mechanical properties measurements and a computational study. Since the MAST program was down-scoped by one-third of the original effort, only the inert propellant development was retained so that a partial crosslink density study could be carried out.

Statement of Work – No. 1

1. General

1.1 Title

Inert hydroxl-terminated polybutadiene solid propellant production, specimen preparation, aging and material property characterization

1.2 Objective

The objective of this statement of work is to obtain services needed to support the Micron Subtopic 5 – Sensor technology development proposal for the AFRL BAA MAST CALL 3 (BAA-RQR-2014-0002). Tasks include:

1. Producing a quantity of inert hydroxyl-terminated polybutadiene (HTPB) propellant with oxidation enhancer;
2. Artificially aging a quantity of inert HTPB propellant;
3. Fabricating test specimens of virgin and aged inert HTPB propellant;
4. Characterizing inert HTPB propellant specimens through uniaxial and Dynamic Mechanical Analysis (DMA).
5. Processing test data to determine mechanical properties and crosslink density.

1.3 Background

The Air Force Research Laboratory Rocket Propulsion Division has the goal of developing technologies to meet the Rocket Propulsion of the 21st Century (RP21) Aging and Surveillance (A&S) objectives. The technologies should increase the Air Force's (AF) ability to detect, predict and/or understand aging that takes place in solid rocket motors (SRM). The technology areas of interest are physics-based modelling, non-destructive

evaluation (NDE) material property investigations, enhanced NDE systems, and solid rocket motor (SRM) sensor technologies.

Micron Instruments has extensive experience and expertise in the development, fabrication and application of high stability, high gain, low power semi-conductor strain gages. Micron believes it can provide technology that can meet the AFRL A&S objectives. To do so, Micron requires the capabilities of a solid propellant rocket motor manufacturer to supply services and materials to support its development efforts.

1.4 Acronyms

AFRL: Air Force Research Laboratory
A&S: Aging and surveillance
AP: Ammonium perchlorate
BAA: Broad agency announcement
DMA: Dynamic mechanical analysis
HTPB: Hydroxl-terminated polybutadiene
KCl: Potassium chloride
NDE: Non-destructive evaluation
POC: Point of contact
SRM: Solid rocket motor

2. SCOPE OF WORK

Task 1 – Production of bulk inert HTPB propellant
The purpose of this task is to produce a bulk quantity of inert HTPB propellant that will meet the needs of the program.

1.1 Produce five (5) US gallons of (NH4)2SO4-HTPB inert solid propellant. Particle size of (NH4)2SO4 should match standard particle distribution of AP particles as much as possible. Appropriate type and quantity of plasticizer, curing agent, stabilizer and crosslinking agent should be used. Ferric oxide nano-particles may be added to enhance oxidation rate.

1.2 Dimensions of bulk propellant container(s) should be appropriate for fabrication of test specimens identified in Task 3 with minimum wastage.

Task 2 – Artificial aging of propellant
The purpose of this task is to artificially age the bulk inert propellant through storage at elevated temperatures.

2.1 Separate the bulk propellant into smaller packages matched to specimen type and aging time as identified by Table 1.

2.2 Wrap the specimen material in packaging to protect from physical damage if necessary. Ensure there is no obstruction to air circulation around the propellant. Identify each pack according to the label given in Table 1.
2.3 Store the specimen packs in a thermal conditioning chamber that is able to maintain 140 F +/- 2 F for the aging times given in Table 1.
2.4 Monitor oxidation rate using Shore A measurements on a weekly basis.
2.5 Ideally, aging over 16 week period will produce a minimum of a three (3) times increase in tensile modulus as measured with a JANNAF specimen.

Table 1 – Specimen-accelerated aging pack identification

	Specimen Type			
Aging Time	**Uniaxial**	**DMA-Prony**	**DMA-Xlink**	**M-DMA**
virgin	0-U	0-DMA-P	0-DMA-X	0-DMA-M
4 weeks	4-U	4-DMA-P	4-DMA-X	4-DMA-M
8 weeks	8-U	8-DMA-P	8-DMA-X	8-DMA-M
12 weeks	12-U	12-DMA-P	12-DMA-X	12-DMA-M
16 weeks	16-U	16-DMA-P	16-DMA-X	16-DMA-M
Legend Uniaxial – JANNAF uniaxial tensile specimen DMA-Prony – DMA specimens to construct relaxation modulus Prony series DMA-Xlink – DMA specimens to measure crosslink density (Xlink) M-DMA – Micron DMA specimens to measure crosslink density				

Task 3 – Test specimen production

The purpose of this task is to fabricate the required type and number of test specimens at the end of each artificial aging period.

3.1 Fabricate the test specimens according to Table 2.
3.2 Wrap the test specimens and surplus propellant in moisture resistant packaging and include desiccant packs with the storage container.
3.3 Store test specimens at 70 F +/- 5 F until needed.

Table 2 – Specimen dimensions and quantity

Specimen	Dimensions (in. x in. x in.)	Quantity
Uniaxial JANNAF	5 x 1 x 0.5 +/- 0.05 in.	50
DMA-Prony	2.5 x 0.5 x 0.25 +/- 0.004 in.	10
DMA-Xlink	2.5 x 0.5 x 0.25 +/- 0.004 in.	10
M-DMA	1 x 1 x 0.5 thk +/- 0.05 in.	20
Notes: DMA specimen dimensions for Prony and Xlink testing will depend on equipment available to the contractor. Specimens must be machined. Quantities listed include extra specimens for preliminary tests.		

Task 4 – Mechanical property characterization

The purpose of this task is to measure the inert HTPB propellant mechanical properties.

4.1 Carry out the property tests identified in Table 3.

4.2 Data to be recorded digitally in data files and plotted graphically for reporting purposes.

Table 3 – Mechanical property test method

Specimen	Test Method	Replicates
Uniaxial	JANNAF uniaxial tensile testing under the following conditions: -40C @ 50mm/min, +20C @ 50mm/min, +60C @ 50mm/min	7 at each temperature
Uniaxial	JANNAF uniaxial tensile testing in a dilatometer cell at +20C @ 50mm/min, virgin material only	7
DMA-Prony	Test method to be confirmed. Generally, frequency sweep at the following isothermal temperatures: - 65C, - 55C, - 45C, - 30C, - 15C, 0 C, +15C, +20C, +30C, +45C, +60C	3
DMA-Xlink	Test method to be confirmed. Generally, temperature sweep from -65C to +60C.	3

Task 5 – Data reduction
The purpose of this task is to reduce the collected property data and to produce material test reports.

5.1 Reduce the data to produce the results identified in Table 4.

5.2 Results shall be available in digital format.

Table 4 – Mechanical property test results

Specimen	**Test Results**
Uniaxial JANNAF	Average and standard deviation for Young's modulus, strain @ max. stress, max. stress, strain @ ult. stress, ult. stress
Uniaxial JANNAF	Average and standard deviation for Young's modulus, strain @ max. stress, max. stress, strain @ ult. stress, ult. stress, change in volume versus strain
DMA-Prony	Graphs of storage and loss moduli and tan delta for test temperatures: - 65C, - 55C, - 45C, - 30C, - 15C, 0 C, +15C, +20C, +30C, +45C, +60C
DMA-Xlink	Graph of storage and loss moduli and tan delta at constant strain level and frequency from -65C to +60C.

3. REPORTS AND OTHER DELIVERABLES

3.1 General

All deliverables shall be delivered in electronic format in two (2) copies on a CD, DVD or USB key as well as:

- All documentation created or received in connection with evaluations or development that could not be included in the report;
- All releasable self-contained code used in the execution of the contract; and
- All billable items purchased in connection with the project.

Final report must include information on:

- Task objective
- Background
- Propellant production
- Test specimen fabrication
- Mechanical property characterization
- Mechanical property results
- Summary and recommendations

Task 1 – Production of bulk inert HTPB propellant
The deliverables for this task include:
- Five (5) US gallons of (NH4)2SO4-HTPB inert solid propellant.

Task 2 – Artificial aging of propellant
The deliverables for this task include:
- Virgin and artificially aged test specimens packaged in moisture resistant wrap per item 2.2 and 2.3 and Table 1.

Task 3 – Test specimen production
The deliverables for this task include:
- Requisite quantity of fabricated test specimens per item 3.2 and Table 2.

Task 4 – Mechanical property characterization
The deliverables for this task include:
- Raw data in digital and graphical format from material characterization tests per Table 3.

Task 5 – Data reduction
The deliverables for this task include:
- Analysis of material property test data per Table 4.
- Results for material property tests.

4. MEETINGS

4.1 Kick-off meeting

Once the contract is activated, the contractor must prepare for and attend a kick-off meeting with Micron Instruments. The meeting must be held in person, at a location agreed upon with the technical and program management points of contact (POC).

4.2 Progress review meetings

Progress review meetings shall be conducted at regular intervals during the contract period via audio conference. The interval period will be determined during the kick-off meeting. The contractor will be responsible for leading these meetings, including preparing the agenda, minutes and follow-up. All progress meetings shall, at minimum, cover the following topics:

- Discussion of progress, results, problems and next steps;
- Management report by the contractor (finances and labour).

5. MICRON SUPPLIED MATERIAL

N/A

6. CONTRACTOR SUPPLIED MATERIAL

Depending on the contractor's requirements and upon approval by the technical point of contact (POC), the contractor may acquire equipment (electronic or mechanical parts, tools, etc.) up to a maximum amount of 5% of the value of the contract. All equipment acquired will remain the property of Micron Instruments upon completion of the contract. All hardware purchases must first be approved by the technical POC.

7. SPECIAL CONSIDERATIONS

N/A

8. WORK SITE

The tasks defined in this SOW shall be performed at the contractor's facilities.

ADDITIONAL INFORMATION

1. Duration of contract

From the contract award date to TBD end date.

2. Technical Point of Contact

Dr. Franklin Wong
Micron Instruments
4509 Runway St.
Simi Valley, CA
USA, 93063
Telephone: 805-522-4676
Fax: 805-522-4982
Email: fwong@microninstruments.com

3. Program Management Point of Contact

Mr. Jim Fillerup
Micron Instruments
4509 Runway St.
Simi Valley, CA
USA, 93063

Telephone: 805-522-4676
Fax: 805-522-4982
Email: jf@microninstruments.com

Statement of Work – No. 2

1. General

1.1 Title

Sensitivity of stress analysis results to crosslink density data

1.2 Objective

The objective of this statement of work is to obtain services needed to support the Micron Subtopic 5 – Sensor technology development proposal for the AFRL BAA MAST CALL 3 (BAA-RQR-2014-0002). Tasks include:

a) Carrying out a parametric analysis of a solid propellant to examine the sensitivity of the stress and strain results of a crosslink density-based constitutive model to changes in crosslink density;
b) Predicting uniaxial stress-strain behavior using measured solid propellant characterization data.

1.3 Background

The Air Force Research Laboratory Rocket Propulsion Division has the goal of developing technologies to meet the Rocket Propulsion of the 21st Century (RP21) Aging and Surveillance (A&S) objectives. The technologies should increase the Air Force's (AF) ability to detect, predict and/or understand aging that takes place in solid rocket motors (SRM). The technology areas of interest are physics-based modelling, non-destructive evaluation (NDE) material property investigations, enhanced NDE systems, and solid rocket motor (SRM) sensor technologies.

Micron Instruments has extensive experience and expertise in the development, fabrication and application of high stability, high gain, low power semi-conductor strain gages. Micron believes it can provide technology that can meet the AFRL A&S objectives. To do so, Micron requires the capabilities of a solid propellant rocket motor manufacturer to supply analysis services to support its development efforts.

1.4 Acronyms

AFRL: Air Force Research Laboratory
A&S: Aging and surveillance
DMA: Dynamic mechanical analysis
HTPB: Hydroxl-terminated polybutadiene
NDE: Non-destructive evaluation
POC: Point of contact
SRM: Solid rocket motor
WLF: Williams Landel Ferry

2. SCOPE OF WORK

Task 1 – Parametric stress analysis based on crosslink density
The purpose of this task is to carry out a parametric stress analysis of a solid propellant to examine the sensitivity of the solution to changes in crosslink density. It is assumed that the contractor has developed a finite element or analytical constitutive model that includes crosslink density as an input parameter.

1.1 Define the uniaxial stick geometry.
1.2 Review material property data set. It is assumed an inert HTPB propellant will be characterized. Table 1 lists the type of property data that will be available. Micron will calculate the Prony series and WLF constants from the DMA data and provide the results to the contractor. Table 2 lists the virgin and aged property data that will be available.

Table 1 – Mechanical property test results

Specimen	**Test Method**	**Replicates**
Uniaxial	JANNAF uniaxial tensile testing under the following conditions: -40C @ 50mm/min, +20C @ 50mm/min, +60C @ 50mm/min	7 at each temperature
DMA-Prony*	Test method to be confirmed. Generally, frequency sweep at the following isothermal temperatures: - 65C, - 55C, - 45C, - 30C, - 15C, 0 C, +15C, +20C, +30C, +45C, +60C	3
DMA-Xlink	Temperature sweep from -65C to +60C.	3
* Micron will provide the Prony series and WLF constants derived from the DMA data.		

Table 2 – Specimen-accelerated aged property data

	Specimen Type			
Aging Time	**Uniaxial**	**DMA-Prony**	**DMA-Xlink**	
virgin	0-U	0-DMA-P	0-DMA-X	
4 weeks	4-U	4-DMA-P		
8 weeks	8-U	8-DMA-P		
12 weeks	12-U	12-DMA-P		
16 weeks	16-U	16-DMA-P		
Legend Uniaxial – JANNAF uniaxial tensile specimen DMA-Prony – DMA specimens to construct relaxation modulus Prony series DMA-Xlink – DMA specimens to measure crosslink density (Xlink)				

1.3 Develop parametric analysis rationale and analysis matrix. Range of crosslink density values shall be selected by the contractor.
1.4 Carry out analysis and summarize results.

Task 2 – Predict stress-strain behavior using measured property data
The purpose of this task is to predict the stress-strain behavior of the uniaxial stick geometry using the measured crosslink density data and to compare the predicted results to the measured uniaxial results.

2.1 Using the Prony series and WLF data (4-DMA-P) and crosslink density data (4-DMA-X) corresponding to the 4 week accelerated aged condition (see Table 3), predict the uniaxial stress-strain behavior at -40C, +20C and +60C.
2.2 Compare the predicted uniaxial results with the measured uniaxial results (identifier 4-U).
2.3 Repeat items 2.1 and 2.2 for the aged conditions 8, 12 and 16 weeks.
2.4 Summarize the results in tables and graphs.
2.5 Provide explanations for observed similarities and differences between the predicted and measured results.

Table 3 – Complete specimen-accelerated aged property data set

	Specimen Type			
Aging Time	**Uniaxial**	**DMA-Prony**	**DMA-Xlink**	
virgin	0-U	0-DMA-P	0-DMA-X	
4 weeks	4-U	4-DMA-P	4-DMA-X	
8 weeks	8-U	8-DMA-P	8-DMA-X	
12 weeks	12-U	12-DMA-P	12-DMA-X	
16 weeks	16-U	16-DMA-P	16-DMA-X	
Legend Uniaxial – JANNAF uniaxial tensile specimen DMA-Prony – DMA specimens to construct relaxation modulus Prony series DMA-Xlink – DMA specimens to measure crosslink density (Xlink)				

3. REPORTS AND OTHER DELIVERABLES

3.1 General

All deliverables shall be delivered in electronic format in two (2) copies on a CD, DVD or USB key as well as:

- All documentation created or received in connection with evaluations or development that could not be included in the report; and

Final report shall include information on:

- Task objective
- Background
- Summary of constitutive model
- Parametric study rationale
- Predicted uniaxial behavior
- Comparison between predicted and measured results
- Summary and recommendations

Task 1 – Parametric stress analysis based on crosslink density

The deliverables for this task include:

- Parametric analysis rationale.
- Predicted uniaxial stress-strain behavior based on contractor selected range of crosslink density.

Task 2 – Predict stress-strain behavior using measured property data

The deliverables for this task include:

- Predicted uniaxial stress-strain behavior for conditions shown in Table 3.
- Comparison of predicted and measured stress-strain results.
- Explanations for observed similarities and differences between the predicted and measured results

4. MEETINGS

4.1 Kick-off meeting

Once the contract is activated, the contractor must prepare for and attend a kick-off meeting with Micron Instruments. The meeting must be held in person, at a location agreed upon with the technical and program management points of contact (POC).

4.2 Progress review meetings

Progress review meetings shall be conducted at regular intervals during the contract period via audio conference. The interval period will be determined during the kick-off meeting. The contractor will be responsible for leading these meetings, including preparing the agenda, minutes and follow-up. All progress meetings shall, at minimum, cover the following topics:

- Discussion of progress, results, problems and next steps;
- Management report by the contractor (finances and labour).

5. MICRON SUPPLIED MATERIAL

N/A

6. CONTRACTOR SUPPLIED MATERIAL

N/A

7. SPECIAL CONSIDERATIONS

N/A

8. WORK SITE

The tasks defined in this SOW shall be performed at the contractor's facilities.

ADDITIONAL INFORMATION

1. Duration of contract

From the contract award date to TBD end date.

2. Technical Point of Contact

Dr. Franklin Wong
Semiconductor Production Manager and Principal Scientist
Micron Instruments
4509 Runway St.
Simi Valley, CA
USA, 93063
Telephone: 805-522-4676
Fax: 805-522-4982
Email: fwong@microninstruments.com

3. Program Management Point of Contact

Mr. Jim Fillerup
Micron Instruments
4509 Runway St.
Simi Valley, CA
USA, 93063
Telephone: 805-522-4676
Fax: 805-522-4982
Email: jf@microninstruments.com

ANNEX B – iMICRO COMPONENT LIST

This Annex details the Nanomechanics Part Numbers that comprise the iMicro instrument.

Notes/Remarks

KLA Corporation and its subsidiaries reserve the right to manufacture and/or deliver all or any part of a Customer's order from any applicable KLA Corporation manufacturing facility or facilities, including but not limited to KLA-Tencor Singapore's manufacturing facility in Singapore.

Item	Part Number	Description	Qty	UOM	Scheduled Ship Date	Extended Price
10	0753157-000	BASE, IMICRO	1	EA	03/30/2020	61,060.00
		equates to P/N 0751976-000				
		Item Net Value				61,060.00
20	0753164-000	InForce 1000 FOR iMicro	1	EA	03/30/2020	24,080.00
		Item Net Value				24,080.00
30	0731270-000	Power Cord - US, CA	1	EA	03/30/2020	
40	0753191-000	SW LIC ADV DYNAMICS CONT. CSM	1	EA	03/30/2020	17,200.00
		Item Net Value				17,200.00
50	0753199-000	SW PK,ProbeDMA POLYMER,AMBIENT	1	EA	03/30/2020	6,450.00
		Item Net Value				6,450.00
60	0753177-000	HOT STAGE, 300C, iMicro	1	EA		51,600.00
		Item Net Value				51,600.00
70	0753180-000	ACTIVE VIBRATION ISOL. TABLE	1	EA	03/30/2020	8,600.00
		Item Net Value				8,600.00
80	0753192-000	SW LIC, USER MTHD DEV. InView	1	EA	03/30/2020	12,040.00
		Item Net Value				12,040.00
90	0731444-000	D2T, CylP, Dia, 100um Flat	1	EA	03/30/2020	3,882.90
		Item Net Value				3,882.90
100	0731445-000	D2T, CylP, Dia, 200um Flat	1	EA	03/30/2020	3,882.90
		Item Net Value				3,882.90
110	0731536-000	XPT, Sphere, Sapp, D158um	1	EA	03/30/2020	2,285.02

Item	Part Number	Description	Qty	UOM	Scheduled Ship Date	Extended Price
						---
		Item Net Value				2,285.02
120	0731537-000	XPT, Sphere, Sapp, D300um	1	EA	03/30/2020	2,076.00

		Item Net Value				2,076.00
130	WRT-01	Regular Warranty (12 months) Coverage is 8 hours per day, 5 days per week, Monday thru Friday. 72 business hours onsite response time. 90% In Country for Planning Networks' Product Lines All Parts Included All Labor Included Holiday coverage not included.	1	EA	03/30/2020	
		Validity Period	12	Months		
150	0731285-000	3 Days of Installation/Training	1	EA	03/30/2020	10,500.00

		Item Net Value				10,500.00
160	0711663-000	FREIGHT CHARGES	1	EA	03/30/2020	300.00

		Item Net Value				300.00
					Sub Total	203,956.82
					Tax	14,003.87
					Total	217,960.69

ANNEX C – FILLED-HTPB DATA

The author carried out a dynamic mechanical analysis (DMA) study on a filled-HTPB material prior to this study. The data was collected using a Rheometrics RSA II instrument in torsion mode. Table C.1 lists the test conditions.

Table C.1 – DMA Test Conditions

Parameter	**Value**
Specimen dimensions (mm)	50 L x 12 W x 4 T
Strain (%)	1
Frequency (r/s)	0.01 to 100
Temperature (C)	−65 to +60

Figure C.1 shows the unshifted storage modulus as a function of frequency and temperature.

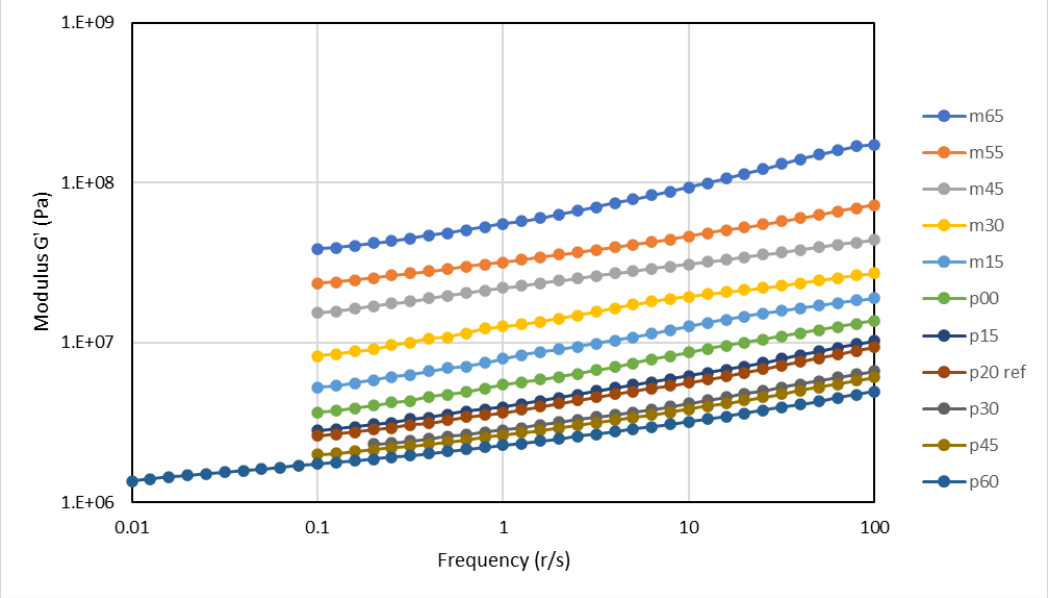

Figure C.1 – Storage modulus of filled-HTPB solid.

Figures C.2 and C.3 show the shifted data and Williams-Landry-Ferry[2] (WLF) shift factors, respectively. The WLF factors were determined to be C_1 = 6.9579, C_2 = 171.97, T_{ref} = 293.4 K.

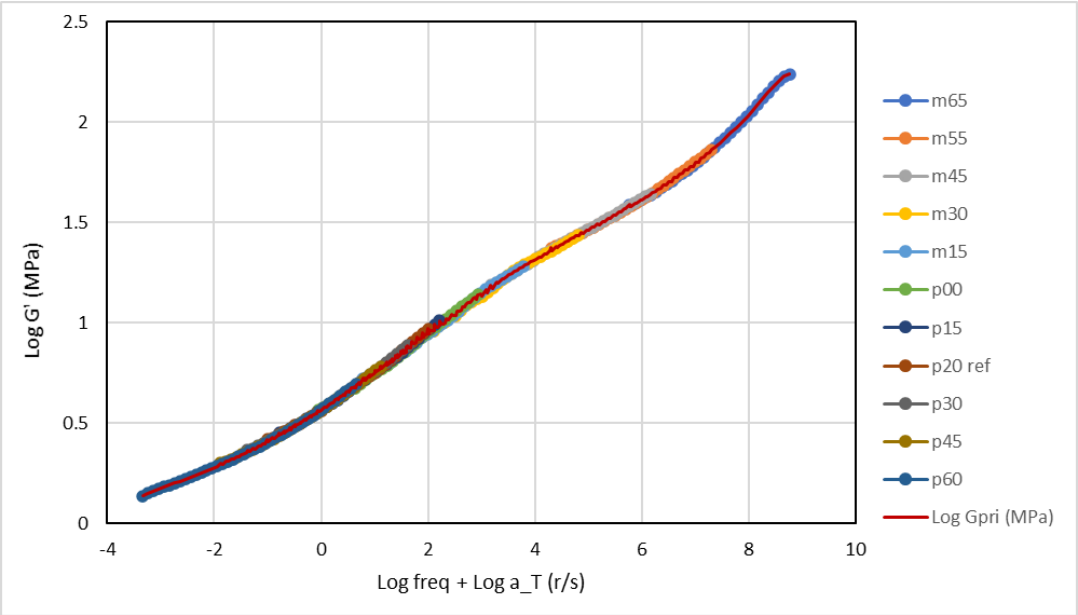

Figure C.2 – Master curve of filled-HTPB in the frequency domain.

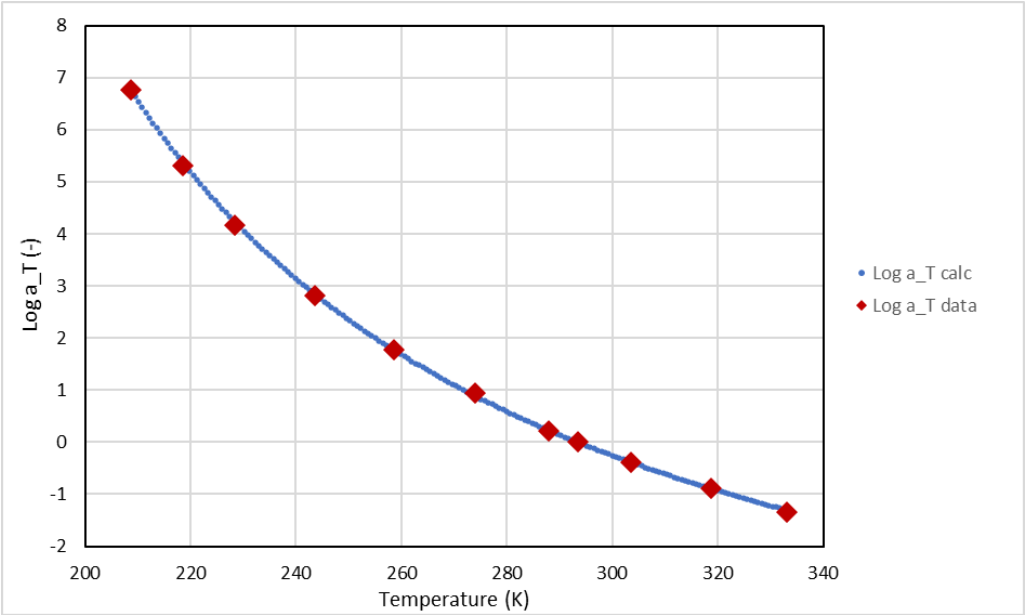

Figure C.3 – WLF shift factors for filled-HTPB.

[2] https://en.wikipedia.org/wiki/Time%E2%80%93temperature_superposition, accessed 22 Jan., 2021.

The frequency-storage modulus data was transformed into the time domain using numerical techniques similar to that used by Zhang[3]. The graphical results are shown in Figure C.4. The Prony-series coefficients are listed in Table C.2.

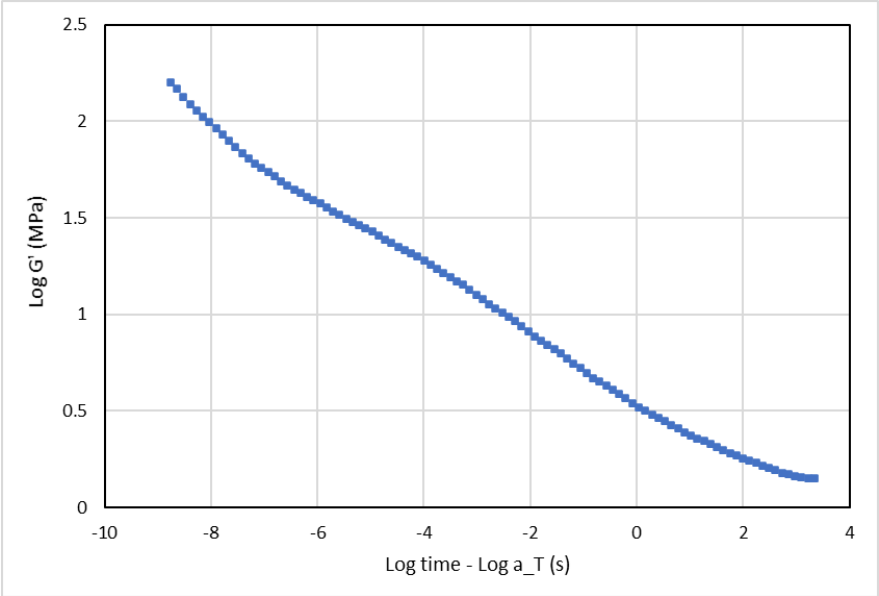

Figure C.4 – Master curve of filled-HTPB in the time domain.

Table C.2 – Prony-Series for filled-HTPB Master Curve

Time Constant, τ_i (s)	**Coefficient, α_i (MPa)**
1.7222037418279366E-009	109.69828475900243
1.4694335459090142E-008	55.303042663830986
1.2537627769586305E-007	23.530690260082533
1.0697463013984746E-006	13.151529237078460
9.1273817534421659E-006	9.0627985538472551
7.7877434644232349E-005	6.9332095398998543
6.6447257171854831E-004	6.0201502613551297
5.6694702462051598E-003	4.0475331202922478
4.8373543530131458E-002	2.7702361196824401
0.41273692462321215	1.6707130334688116
3.5215896234956712	0.96273779189178299
30.047211035537487	0.58504719176884512
256.37140823862717	0.42930211727585177
Equilibrium modulus is 1.3684999900000001 (MPa)	

[3] Zhang, W., Cui, B., Gu, X., Dong, Q., 'Comparison of Relaxation Modulus Converted from Frequency- and Time-Dependent Viscoelastic Functions through Numerical Methods', Appl. Sci., 2018, Vol. 8, pp. 2447-2461.

LIST OF ACRONYMS

CIW	Confidence Interval Width
DMA	Dynamic Mechanical Analysis
HTPB	Hydroxyl-Terminated Polybutadiene
PLI	Propellant Liner Interface
NBR	Nitrile Rubber
NGIS	Northrop Grumman Innovation Systems
NR	Natural Rubber
NSST	Normal-Shear Stress and Temperature sensor
SAM	Sensor Application and Modelling
SBR	Styrene-Butadiene Rubber
SLE	Service Life Estimate
SRM	Solid Rocket Motor
TMXDI	Tetramethyl-xylene Diisocyanate

This page intentionally left blank.